理學碩士 學位論文

수소화물 기상 에피탁시법을 이용한 극성/비극성 GaN 후막의 구조적 결함 감소에 관한 연구

A Study on the Reduction of Structural Imperfections in Polar/Non-polar GaN Thick Films Grown by Hydride Vapor Phase Epitaxy

指導交綏 張 志 豪

2012年 2月

韓國海洋大學校 大學院

應用科學科 半導體物理專攻

趙 英 志

本 論文을 趙英志의 理學碩士 學位論文으로 認准함

위원장   安 亨 秀   (인)

위 원   李 三 寧   (인)

위 원   張 志 豪   (인)

2012년 2월

한국해양대학교 대학원

Contents

Chapter 3. HVPE Growth of reduced defect density polar GaN

Chapter 4. HVPE Growth of reduced defect density nonpolar GaN

References

Figure list

Chapter 1

Chapter 2

Chapter 3

Chapter 4

Table list

논 문 요 약

본 논문에서는 III-V족 화합물 반도체인 GaN를 HVPE 방법으로 성장시킬 때 내부의 결함을 감소시키는 방법들을 제시하였고, 그 방법으로 성장한 GaN film의 구조 및 광학적 특성 조사를 통하여 고품질의 GaN 후막 제작에 대한 가능성을 고찰하였다. 이 논문의 목적은 기존에 사용해오던 사파이어 기판과의 커다란 부 정합 차에 의하여 고품질의 성장이 제한되었던 GaN 이종 성장 시 중온에서 성장한 버퍼층을 삽입함으로써 GaN 후막의 결정성을 향상시키는 것뿐 만 아니라, 최근 주목 받고 있는 비극성 GaN의 최대 문제점인 적층 결함을 기울어진 기판의 사용을 통해 감소시킴으로써 고품질의 후막을 얻을 수 있는 가능성을 보여줌에 있다. 본 논문은 총 5장으로 구성되어 있으며 각 장의 내용은 다음과 같다

제 1장에서는 기본적인 GaN 물성과 그를 이용한 여러 응용 분야 및 최근 주목 받는 비극성 GaN에 대해 소개하고 종래의 GaN 이종성장이 가지고 있는 문제점과 그 해결 방법으로 주목 받고 있는 HVPE 후막 GaN 성장에 대하여 설명했다. 제 2장에서는 GaN 후막을 성장 및 평가하기 위해 본 연구에서 사용된 방법인, HVPE, PL, CL, TEM, XRD 에 대하여 정리했으며 GaN 특성에 큰 영향을 미치는 내부 결함에 대해서도 조사하였다. 제 3장은 900°C의 온도에서 성장한 중온 버퍼를 사용하여 고품질의 GaN 후막을 성장한 후 그 중온 버퍼가 GaN 후막 결정성 향상

에 있어 어떤 역할을 하는지 고찰해보았다. 제 4장은 비극성 *m*-plane GaN 성장 시 여러 방향으로 기울어진 *m*-plane sapphire 기판들을 사용하였고, 그 중 적층 결함의 밀도가 가장 많이 감소하는 기울기 방향을 찾아내었다. 그리고 그 이유를 atomic-bond 모델을 통해 설명했다. 마지막으로 제 5장에서는 본 논문에서 얻은 결과를 정리하여 결론을 기술하였다.

Abstract

In this thesis, the techniques to grow high quality HVPE GaN film with low defects density were suggested and discussed. The objectives of his thesis are to improve the crystalline of GaN film by using buffer layer grown at intermediate temperature and to grow high quality non-polar GaN films with low stacking faults density by using vicinal substrates.

In the chapter 1, the fundamental GaN properties, applications of GaN, nonpolar GaN and problems in hetero epitaxial GaN growth are introduced. In the chapter 2, the principles of hydride vapor phase epitaxy (HVPE), photoluminescence (PL), cathodoluminescence (CL), transmission electron microscopy (TEM), x-ray diffraction (XRD) and defects in GaN crystal are explained. In the chapter 3, high quality GaN film grown by using intermediate buffer layer grown at 900°C (IT-GaN) is investigated and the role of IT-GaN on the improvement of GaN crystalline is discussed. In the chapter 4, it is discussed that the structural and optical properties of m-plane GaN (m-GaN) films are affected by the inclination direction of vicinal m-plane sapphire substrate. And it is founded that inclined in the a-axis direction showed the highest quality with a smooth surface and a low stacking fault density. A model is proposed that shows how the surface step of a substrate can reduce the generation of stacking fault in m-GaN film. Finally, the results found from this thesis are summarized and concluded in the chapter 5.

Chapter 1. Introduction

1-1. Properties of GaN

Gallium nitride (GaN) is an attractive material due to its interested properties. GaN and other III-nitrides are special among the other III-V compounds (such as GaAs or InP) as this has a strong effect on their properties due to the involvement of nitrogen, which is the smallest and the most electronegative Group V element. Because of the $1s^2 2s^2 2p^3$ electronic configuration of the N atom, or rather the lack of electrons occupying the outer orbitals, the electrons involved in the metal-nitrogen covalent bond will be strongly attracted by the Coulomb potential of the N atomic nucleus. This means that this covalent bond of GaN will have stronger ionicity compared to other III-V covalent bonds. This is closely related to why GaN has a high melting point, thermal and chemical stability, wide band-gap and high thermal conductivity as shown in TABLE 1.1. And these are special properties for applications in optoelectronic, high-power and high-frequency devices [1-3]. Furthermore, the bandgap of Al-Ga-In-N system can be tunable over the range 0.65 – 6.2 eV, from infra-red to the ultraviolet, encompassing the entire visible spectrum, as shown in the Fig. 1.1 below comparing the lattice constant to the room temperature bandgap of many compounds [4,5]. Therefore, these III-nitrides materials have good advantages to apply optical devices, also, the development of GaN-based optical devices is expected to have an enormous effect on display and lighting technology.

TABLE 1.1 Material properties of GaN.

Properties		Value
RT (300K) energy		3.44
Lattice constant	a (Å)	3.18843
	c (Å)	5.18524
Density (g/cm^2)		6.15
Coefficient of thermal expansion at 300K	a (10^{-9}/K)	5.59
	c (10^{-9}/K)	3.17
Thermal conductivity at 300K (W/cm•^{o}C)		> 2.1
Infrared refractive index		2.3
Electron affinity (eV)		3.4
Heat capacity at 300K (J/mol•/k)		35.3
Group of symmetry		C6$_3$mc
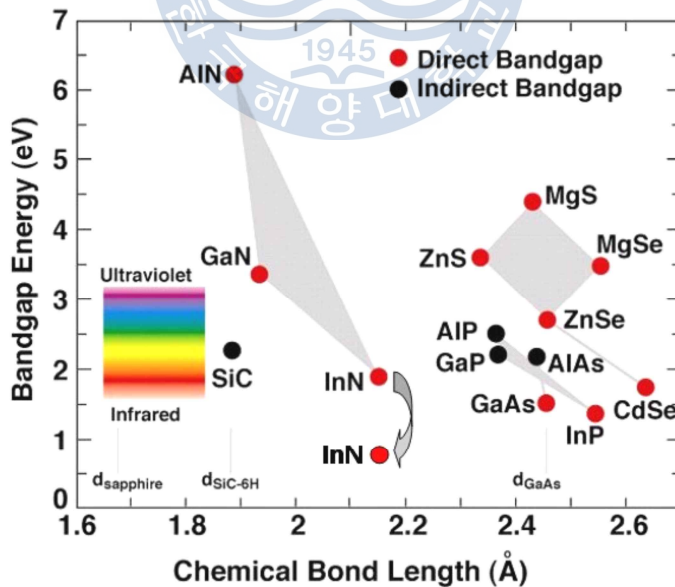
Fig. 1.1 Bandgap energy versus lattice constant of III-V nitride semiconductors at room temperature.

5

Without LT - buffer
Before 1985

With LT-buffer
Since 1986

NAGOYA UNIV.

Many cracks, Pits   ⟶ Crack-free, Pit-free
Rough surface   ⟶ Specular surface
Dislocations $> 10^{11} \text{cm}^{-2}$ ⟶ Dislocations $10^8 \sim 10^9 \text{cm}^{-2}$
Electron mobility$\sim 20 \text{cm}^2/\text{v·s}$ ⟶ Electron mobility$\sim 700 \text{cm}^2/\text{v·s}$
Weak luminescence   ⟶ Intense luminescence
                   (Sharp edge emission)
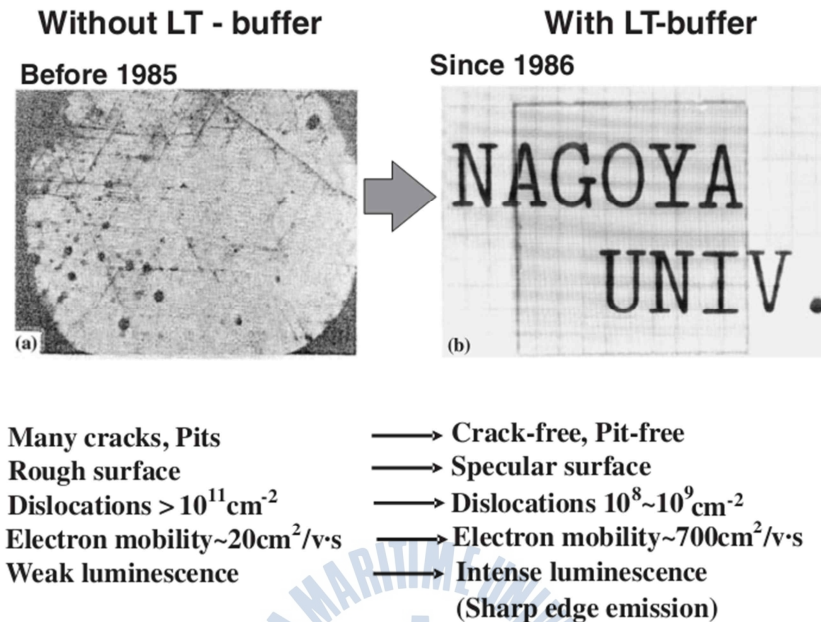
Fig. 1.2 Photographs of GaN films grown on sapphire substrate by MOVPE ;
(a) without and (b) with LT-buffer layer.

1-2. Application of GaN

1-2. 1. High quality polar GaN

The first GaN was synthesized by Johnson et al. in 1932 [6]. Nevertheless GaN has attractive properties to apply devices, the application was started in 1970's [7], because sufficiently high quality crystalline layers were not produced due to lack of homogeneous substrate. The difficulty of growing high quality crystalline films lies in the problem of finding a suitable substrate material. The lattice and thermal coefficient mismatches between substrate and GaN film lead to defects which act as

6

non-radiative recombination centers and reduce the quantum efficiency [8]. Akasaki demonstrated in 1986 [9] that metal organic vapor phase epitaxy (MOVPE) growth of smooth surfaces of GaN films is possible on sapphire using a sequence of buffer layer grown at different substrate temperatures, as shown Fig. 1.2. And then thin AlN or GaN nucleation layers deposited at temperatures between 500 and 750 $^{\circ}$C showed to remarkably improve the quality of the GaN film grown at temperatures above 1000 $^{\circ}$C (Akasaki, et al. 1989 and Nakamura, et al. 1991) [10,11]. These studies promoted the application of GaN-based devices.

1-2. 2. Necessary of Non-polar GaN

The group of III-nitrides AlN, GaN, and InN can crystallize in the following three crystal structures: wurtzite, zinc-blende, and rock-salt. However, at amnient conditions the wurtzite structure is the thermodynamically stable phase consisting of two interpenetrating hexagonal close packed lattices [12]. Most of wurtzite III-nitride based devices have been grown mainly in the (0001), *c*-plane orientation. Because it became relatively easy to grow planar *c*-plane GaN due to its growth stable. Wurtzite is the structure with P6$_3$mc symmetry compatible with the existence of polar [13]. Since the polar symmetry, the III-nitrides of wurtzite structure have a spontaneous polarization along the *c*-axis. Also piezoelectric polarization in III-nitrides follows from the uniaxial lattice geometry of the wurzite lattice structure in combination with partially ionic bonding properties in the diatomic point group that

7

lacks inversion symmetry [14].

Hence heteroepitaxy along the unique *c*-axis induces discontinuities of discontinuities of the polarization component and pseudomorphic-heteroepitaxy adds piezoelectric components due to induced biaxial strain. Follow Fig. 1. 3 shows the effect of strain and the growth face on the direction of the spontaneous and piezoelectric polarization. As a figure, an electric field induced by piezoelectric polarization and spontaneous polarization strongly affect in the optical properties of III-nitrides by the quantum confined Stark effect (QCSE) [15].
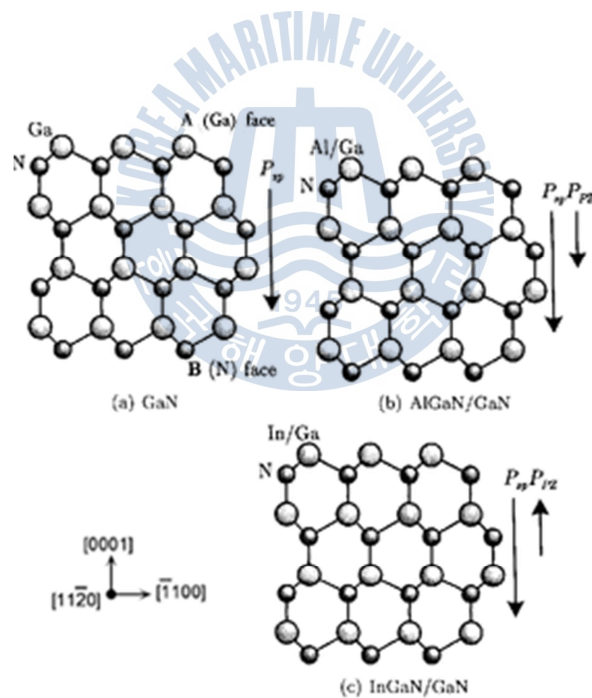
Fig. 1.3 Crystal structures of spontaneous and piezoelectric polarization in nitride materials. (a) unstrained GaN; (b) The A (Ga-terminated) and (c) the C (N-terminated) crystal faces are indicated for GaN.
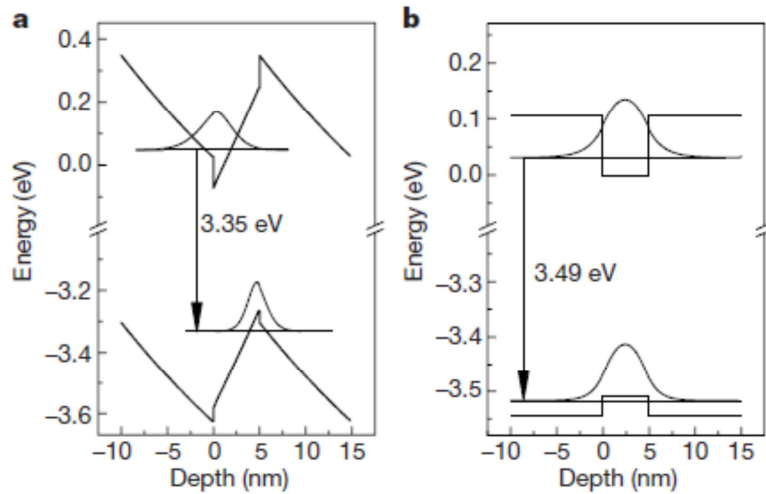
Fig. 1.4 Schematic band structure diagram of GaN/AlGaN QW oriented along different crystal axis. (a) the large electrostatic fields in polar *c*-axis and (b) free of electrostatic fields in the non-polar *m*-axis.

Such polarizations localized within a bipolar LED structure can cause a range of dynamic instabilities when electrons and holes are injected in regular device operation, as Fig. 1.4 (a). The pool electron-hole overlap results in long radiative lifetimes and thus in low internal quantum efficiencies, given that non-radiative recombination is always present at elevated temperature. However, as Fig. 1.4 (b) shown, the polarization effects in III-nitrides can be eliminated by growth of the devices on the non-polar plane of crystals such as *a*-plane (11-20) and the *m*-plane (1-100) of GaN. The *a*- and *m*- plane oriented films have their *c*-axis parallel to their surface, and therefore the growth along the these axis should provide vanishing polarization and a big increase in the interband dipole matrix element and quantum

9

efficiency [16].

1-3. Pending Problem of GaN

1-3. 1. Lack of GaN substrate

1-3. 1. 1. Defect reduction of Hetero epitaxy polar GaN growth

Although GaN substrate is the best as a substrate for GaN epitaxy and device fabrication, heterogeneous substrates have been used. Because GaN has a high melting point and a high equilibrium vapor of nitrogen in GaN. As phase diagram in Fig. 1.5, the melting of GaN happened at about 2,200 °C and at pressures above 6 GPa, and the GaN melt is crystallized with the temperature decrease [17].

Thus, it is too difficult to grow bulk GaN, and the typically GaN film was grown on foreign substrates, such as sapphire [18], SiC(6H) [19] and LiGaO$_2$ [20] etc. as shown in TABLE 1.2. Since the quality of GaN film was improve by the low temperature (LT) AlN and a LT GaN buffer layer between sapphire substrate and epitaxial GaN film, sapphire is the most commonly used substrate in GaN epitaxial growth. However, sapphire has a large lattice misfit over than 16% and a thermal expansion coefficient mismatch with GaN. These mismatches between the sapphire substrate and epitaxial GaN layer easily generate a high density of dislocation in GaN thin films. Although LT buffer layers have contributed improve crystallinity, electrical and optical properties of GaN layers, there are still many obstacles to realize high efficiency devices.

10
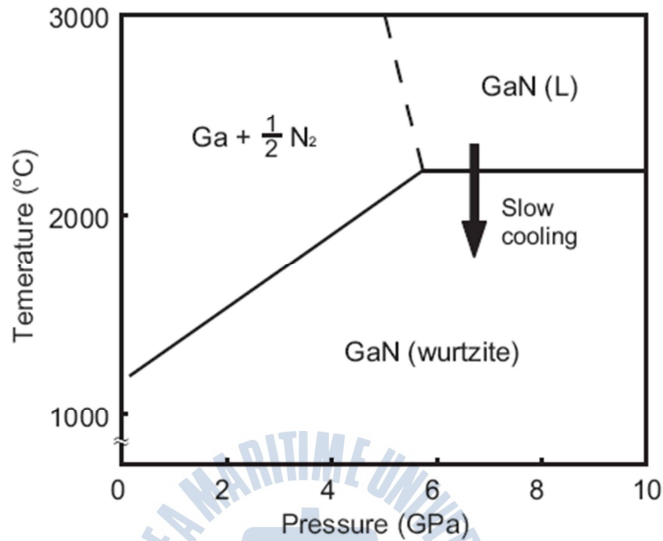
Fig. 1.5 Phase diagram of GaN under high pressure and temperature.

As addressed in section 1-2. 1., misfit defects act as non-radiative recombination centers and reduce the quantum efficiency. Moreover the operation of device is strongly influenced by junction temperature of active-region, and the increased temperature in defects area such as threading dislocation (TD) cause the breakdown or failure of devices [25]. Accordingly, various substrates, such as Si, SiC (6H), and ZnO etc., other buffer layer such as ZnO [26], InN [27] as well as LT buffer layer were suggested as useful technique to grow high quality GaN film with low defects density. But despite a lot of tries, many TDs extend along the c-axis of grown GaN from the interface between the heterogeneous substrate and epitaxial layer.

11

TABLE 1.2 Material properties of substrates for GaN epitaxy.

Crystal	Structure	Lattice misfit [%]	TEC Mismatch [%]	Ref.
GaN	Wurtzite	0	0	[21]
N	Wurtzite	3	33	
Sapphire	Corundum	16	-25	[18]
SiC (6H)	6H Wurtzite	4	24	[19]
Si	Diamond	-17	115	[22]
GaAs	Zncblend	-20	-7	[23]
LiGaO$_2$	Othorhombic	1	-23	[20]
ZnO	Wurtzite	-2	-13	[24]

1-3. 1. 2. Problems of non-polar GaN growth

Non-polar GaN growth is an attractive method for eliminating polarization effect in III-nitrides device. Among the two non-polar planes of GaN, the *a*-plane GaN is usually grown on *r*-plane sapphire. However, the development of *a*-plane GaN has been hindered by low crystalline quality mainly due to basal stacking faults (BSFs) [28]. The *m*-plane GaN is currently grown on γ-LiAlO2 and *m*-plane SiC substrates typically [29,30], which are have restricted crystal quality of grown *m*-GaN and higher cost compared with sapphire substrate. The non-polar GaN

12

grown on heterogeneous substrate have a high density of stacking faults and TDs, which should be limited the device performance.

1-4. Fabrication of pseudo GaN substrate

1-4. 1. HVPE thick GaN growth

GaN substrate is essential to grow high quality GaN film for high efficiency devices. But a bulk GaN ingot has not been produced although bulk GaN growth technique has been researched for a long time. Hence importance of pseudo GaN substrate – thick GaN growth for substrate becomes more significant. Among various growth methods of GaN, thick GaN grown by hydride vapor phase epitaxy (HVPE) is very promising approach for obtaining such substrate. Because the growth rate of GaN in HVPE has reached as high as 100 μm/hr [31], and a bulk-like GaN thickness of several hundred micrometers has been easily gained on 2 inch substrates [32].

Many research groups have studied about the various ways of growing low defect density and crack free GaN by HVPE [33-35]. However, there is a pending issue about the separation of sapphire substrate from the GaN thick layer because it is rigorous and time-consuming process [36], and free-standing GaN easily have crack if thick GaN has strain.

1-4. 2.Other methods

Other methods for thick GaN growth are N_2 high pressure [37], Na-flux [38], liquid phase epitaxy (LPE) [39], and ammonothermal [40], etc. The GaN grown by N_2 high pressure method can be obtain extremely low dislocation density, but it is necessity for high nitrogen pressure (< 10,000 atm) and high growth of temperature (<1,500^{o}C) and it has a low growth rate. The Na-flux method could require lower pressure to grow GaN single crystals in a solution system. However, the growth rate is low and the growth of large-size crystal is difficult. LPE is used GaN template and grown by metal organic chemical vapor deposition (MOCVD). This method can grow larger area GaN, but the growth rate was still low. Ammonothermal method has several advantages for thick GaN growth, which are simple equipment, process scalability, lower process temperatures compared with other thick GaN growth techniques. However, the growth rate is too slow about 50μm per day [41].

1-5. Proposal and purpose of this thesis

1-5. 1. HVPE of polar GaN with reduced defect density

GaN-based optical devices have the critical problems that the efficiency of device decline by the light emission decrease and thermal of electrical damage near defect area as discussed before section. So, high quality GaN crystal with low defects is certainly demanded, and GaN grown on GaN substrate is the best choice

14

for GaN epitaxy and fabrication of devices. The high quality GaN grown by homoepitaxy is not required nitridation or buffer layers as other heterogeneous substrates. Although GaN substrate is suitable for GaN epitaxy, the heterogeneous substrates have been used for GaN epitaxy typically due to difficulty of GaN bulk growth by its high melting point and high pressure of nitrogen. Thus, thick hetero-epitaxial GaN is commonly grown on sapphire substrate by HVPE for producing GaN substrate.

As well known, HVPE GaN is still grown on heterogeneous substrate like sapphire which has large mismatches compared with GaN, and it leads to high density of internal defects. The main defect of polar GaN is threading dislocation (TD) which caused decrease of device efficiency due to non-radiative recombination and leakage current [42,43]. In this thesis, stacking faults are used to reduce TDs. Stacking fault is a planar defect, also it forms while perfect dislocation dissociate into partial dislocation. Therefore a buffer layer which contains stacking faults is expected to reduce TDs efficiently.

1-5. 2. HVPE of non-polar GaN with reduced defect density

Non-polar such as *m*- or *a*-plane nitrides based optoelectronic devices are attractive compared to the *c*-plane devices. Because *c*-plane with polar devices suffer from the quantum-confined Stark effect (QCSE) due to the large electric field from spontaneous and piezoelectric polarization of GaN [14]. These polarizations

15

are intimately related with internal electric field along the *c*-axis that cause the electron-hole separation which result in a reduction of radiative recombination efficiency. Thus using non-polar plane instead of *c*-plane nitrides has a definite advantage by vanishing polarization. However, the development of non-polar nitrides based devices is limited by high density of stacking faults and threading dislocation due to hetero epitaxy. So, the growth of high quality non-polar GaN substrates is more becoming important issue. There are many techniques to grow high quality thick GaN, but the techniques need complex processes. In this thesis, vicinal substrate is used to grow high quality thick GaN. Stacking fault which is main defect of non-polar GaN cause steps of GaN surface. Therefore the vicinal substrate which has surface steps is expected to reduce stacking faults.
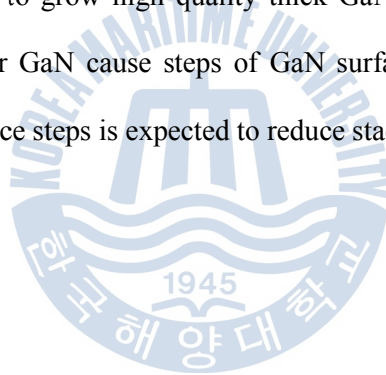
References

[1] S. Nakamura, M. Senoh, S. Nagahama, N. Iwasa, T. Yamada, T. Matsushida, Y. Suhimoto and H. Kiyoku, Appl. Phys. Lett. 69 (1996) 3034.

[2] H. Morkoç, G. S. Strite, G. B. Gao, M. E. Lin, B. Sverdlov and M. Burns, J. Appl. Phys. 76 (1997) 1363.

[3] Y. F. Wu, D. Kapolnet, J. P. Ibbetson, P. Parikh, B. P. Keller and U. K. Mishra, IEEE Electron. Dev. Lett. 48 (2001) 586.

[4] F. A. Ponce and D. P. Bour, Nature 386 (1997) 351.

[5] T. Matsuoka, H. Okamoto, M. Nakao, H. Harima and E. Kurimoto, Appl. Phys. Lett. 81 (2002) 1246.

[6] W. C. Johnson, J. B. Parsons, and M. C. Crew, J. Phys. Chem. 36 (1932) 2651.

[7] J. I. Pankove, E. A. Miller and J. E. Berkeyheiser, J. Lumin. 4 (1971) 63.

[8] M. Albrecht, H. P. Strunk, J. L. Weyher, I. Grzegory, S. Porowski and T. Wosinski, J. Appl. Phys. 92 (2002) 2000.

[9] H. Amano, N. Sawaki, I. Akasaki and Y. Toyoda, Appl. Phys. Lett. 48 (1986) 353.

[10] I. Akasaki, H. Amano, Y. Koide, K. Hiramatsu and N. Sawaki, J. Cryst. Growth 98 (1989) 209.

[11] S. Nakamura, Jpn. J. Appl. Phys. 30 (1991) L1705.

[12] O. Ambacher, J. Phys. D: Appl. Phys. 31 (1998) 2653

[13] L. Filippidis, H. Siegle, A. Hoffmann, C. Thomsen, K. Karch and F. Bechstedt, Phys. Stat. Sol. (b) 198 (1996) 621.

[14] F. Bernardini, V. Fiorentini and D. Vanderbilt, Phys. Rev. B 56 (1997) R10024.

[15] T. Onuma, H. Amaike, M. Kubota, K. Okamoto, H. Ohta, J. Ichihara, H. Takasu and S. F. Chichibu, Appl. Phys. Lett. 91 (2007) 181903.

[16] P. Waltereit, O. Brandt, A. Trampert, H. T. Grahn, J. Menniger, M. Ramsteiner, M. Reiche and K. H. Ploog, Nature Materials 406 (2000) 865.

[17] W. Utsumi, H. Saitoh, H. Kaneko, T. Watanuki, K. Aoki and O. Shimomura, Nature Material, 2 (2003) 735.

[18] B. J. Skromme, H. Zhao, D. Wang, H. S. Kong, M. T. Leonard, G. E. Bulman and R. J. Molnar, Appl. Phys. Lett. 71 (1997) 829.

[19] K. Jeganathan, M. Shimizu and H. Okumura, Phys. Stat. Sol. (c) 0 (2002) 143.

[20] S. Duan, X. Teng, P. Han and D. Lu, J. Cryst. Growth 195 (1998) 304.

[21] N. Preschilla A., S. Major, N. Kumar, I. Samajdar and R. S. Srinivasa, Appl. Phys. Lett. 77 (2000) 1861.

[22] A. Watanabe, T. Takeuchi, K. Hirosawa, H. Amano, K. Hiramatsu and I.

Akasaki, J. Cryst. Growth 128 (1993) 391.

[23] S. Huang, H. Wang, C. Hsu, J. Gong, C. Chiang, S. Tu and H. Chang, J. Mater. Sci. Lett. 17 (1998) 1281.

[24] Y. Izawa, T. Oga, T. Ida1, K. Kuriyama, A. Hashimoto, H. Kotake and T. Kamijoh, Appl. Phys. Lett.99 (2011) 021909.

[25] M. S. Ferdous, X. Y. Sun, X. Wang, M. N. Fairchild and S. D. Hersee, J. Appl. Phys. 99 (2006) 096105.

[26] R.Wang, H. Muto, Y. Yamada and T. Kusumori, Thin Solid Films 411 (2002) 69.

[27] T. Kachi, K. Tomita, K. Itoh and H. Tadano, Appl. Phys. Lett. 72 (1998) 704.

[28] K. H. Baik, Y. G. Seo, S. K. Hong, S. Lee, J. Kim, J. S. Son and S. M. Hwang, IEEE PHOT. TECH. LETT.22 (2010) 595.

[29] P. Waltereita, O. Brandta, M. Ramsteinera, R. Ueckerb, P. Reicheb and K. H. Ploog, J. Cryst. Growth 218 (2000) 143.

[30] M. McLaurin, T. E. Mates, F. Wu and J. S. Speck, J. Appl. Phys. 100 (2006) 063707..

[31] R. P. Vaudo, X. Xu, A. Salant, J. Malcarne and G. R. Brandes , Phys. Stat. Sol. (a) 200 (2003) 18.

[32] T. Paskova, D. A. Hanser and K. R. Evans, Proceedings of the IEEE, 98 (2010)

1324.

[33] C. E. C. Dam, A. P. Grzegorczyk, P. R. Hageman and P. K. Larsen, J. Cryst. Growth 209 (2006) 473.

[34] H. Ashraf, J. L. Weyher, G. W. G. van Dreumel, A. Gzregorzyck and P. R. Hageman, J. Cryst. Growth, 310 (2008) 3957.

[35] H. Huang, K. Chen, L. Tu, T. Chu, P. Wu, H. Yu, C. Chiang and W. Lee, Jpn. J. Appl. Phys. 47 (2008) 8394.

[36] G. Chen, J. Chyi, C. Chan, C. Hou, C. Chen and M. Chang, Appl. Phys. Lett. 91 (2007) 261910.

[37] I. Grzegory, Mater. Sci. Eng. B 82 (2001) 30.

[38] F. Kawamura, H. Umeda, M. Morishita, M. Kawahara, M. Yoshimura, Y. Mori, T. Sasaki and Y. Kitaoka, Jap. J. Appl. Phys. 45 (2006) L1136.

[39] M. Morishitia, F. Kawamura, M. Kawahara, M. Yoshimura, Y. Mori, and T. Sasaki, J. Cryst. Growth 271 (2004) 270.

[40] T. Hashimoto, F. Wu, J. S. Speck and S. Nakamura, Nature Materials 6 (2007) 568.

[41] B. Wang, M. J. Callahan, K. D. Rakes, L. O. Bouthillette, S. -Q. Wang, D. F. Bliss and J. W. Kolis, J. Cryst. Growth 287 (2006) 376.

[42] D. Cherns, S. J. Henley and F. A. Ponce, Appl. Phys. Lett. 78 (2001) 2691

[43] D. S. Li, H. Chen, H. B. Yu, H. Q. Jia, Q. Huang and J. M. Zhou, J. Appl. Phys. 96 (2004) 1111

Chapter 2. Experiment and theoretical background

A. Experiments

i. Hydride Vapor Phase Epitaxy (HVPE)

Developed in the 1960s, it was the first epitaxial method used for the fabrication of single GaN crystals. One of the key features of the technique is its high growth rate (at up to 100 μm per hour) which is almost two orders of magnitude faster than typical metal organic chemical vapor deposition (MOCVD) and molecular beam epitaxy (MBE) processes. The technique is able to produce crack-free, high quality thick GaN epitaxial layers
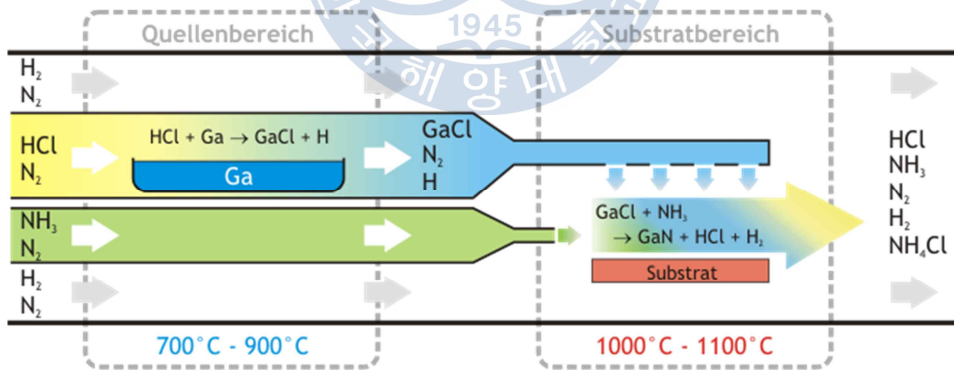
Fig. 2.1 Schematic diagram of HVPE system.

As an epitaxy process that works near thermodynamic equilibrium, it is particular interest for applications such as selective area growth, overgrowth of

buried structures, and planar growth. The opportunity this process offers to efficiently manufacture extremely thick and pure compound semiconductor structures means that ithas been recently used primarily in the manufacture of GaN substrates or templates.

The HVPE is usually carried out in a hot wall reactor, at atmospheric pressure. A novel aspect of this method is that the group III precursors are usually synthesized within the reactor vessel, upstream from the substrate, by either the reaction of a halide containing gas, such as hydrogen chloride (HCl), with a group III metal at high temperature. In the case of GaN, gallium monochloride is usually synthesized upstream in the reactor by reacting HCl gas with liquid Ga metal at 700 - 900 $^{\circ}$C:

$$Ga(l) + HCl(g) \rightarrow GaCl(g) + 1/2\ H_2(g) \text{------------------------------------ (1)}$$
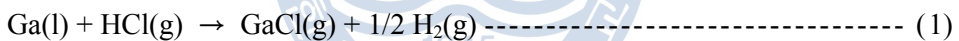
The GaCl is transported to the substrate where it is reacted with NH_3 at 1000 – 1100 $^{\circ}$C to form GaN, via the reaction:

$$GaCl(g) + NH_3 \leftrightarrow GaN(s) + HCl(g) + H_2(g) \text{------------------------------- (2)}$$
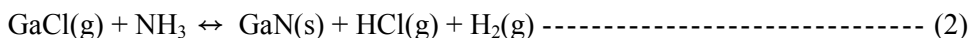
The HVPE process tends to create copious amounts of NH_3Cl and $GaCl_3$. NH_3 is condense on and eventually clog exhaust lines unless they are heated to sufficiently high temperatures and/or operated at reduced pressure.

23

ii. Photoluminescence (PL)

Photoluminescence is a well-established and widely practiced tool for materials analysis due to its sensitivity, simplicity, and low cost. In the context of surface and microanalysis, PL is applied mostly qualitatively or semi quantitatively to exploit the correlation between the structure and composition of material system and its electronic state and their lifetimes, and to identify the presence and type of trace chemicals, impurities, and defects. PL systems and largely made up the source of light for excitation (laser), sample holder (or cryostat to measure at low temperature), including optics for focusing the incident light and collecting the luminescence, filter, a double or a triple monochromator, the optical detector such as photomultiplier tube or CCD or photodiode arrays, and recording equipment. The experimental setup for the PL measurements used in this study is schematically shown in Fig. 2. 2.
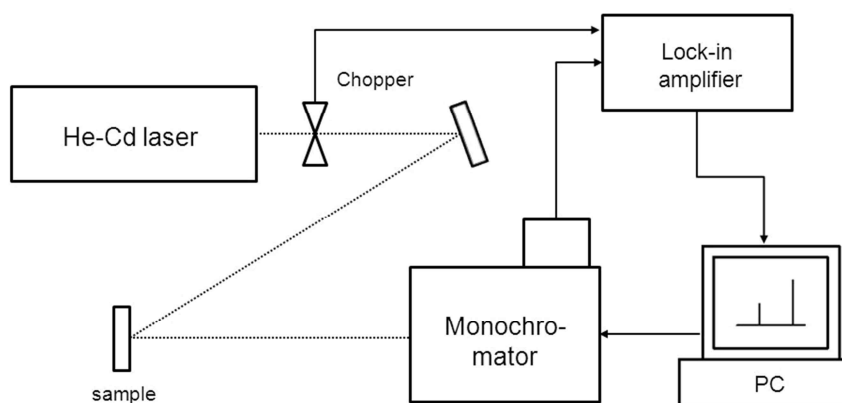
Fig. 2.2 Experimental setup of the PL measurement system.

In PL, a material gains energy by absorbing light at some wavelength by promoting an electron form a low to a higher energy level. This may be described as making a transition from the ground state to an excited state of a semiconductor crystal (electron-hole creation), the system then undergoes a non radiative internal relaxation involving interation with crystalline or molecular vibrational and rotational modes, and the excited electron moves to a more stable excited level, such as the bottom of the conduction band or the lowest vibrational molecular state.

These electrons and holes (carriers) are considered to be in quasi thermal equilibrium states and decay by recombination via several kinds of transitions showed in Fig. 2. 3. Eg means the band-gap of a semiconductor and incident light should have higher energy than this to excite carrier up to conduction band; GaN has approximate 3.39eV of band-gap at room temperature (RT, 300K).

Generally, photoluminescence by (b) is called free-exciton transition and this is dominantly observed peak at RT. (c) and (d) are transitions by exciton bound to neutral acceptor and donor, and (e) and (f) are transitions of (d) and (c) induced by ionized impurities, respectively. Finally, (g) is a transition from a donor to an acceptor level. Above this standard transitions are simply explained. However, there exists more complex kind of peaks in real measurement of PL, due to phonons or impurities.
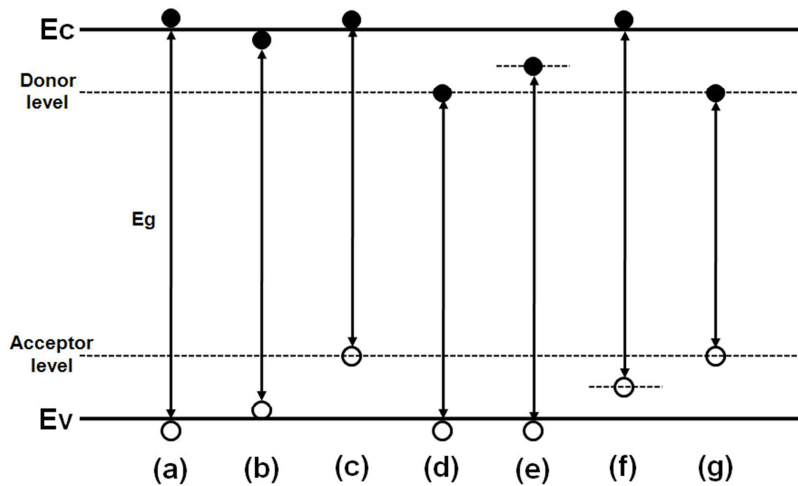
Fig. 2.3 Radiative recombination processes in a semiconductor. Every transition accompanies an emission of energy as a light with different wavelength.

The multitudinous of optical transitions that could be and have been observed in the luminescence spectra of GaN associated with defects was summarized as shown in TABLE 2.1[1]. The list shows a schematic description of the related transitions and energy positions within the gap of the defect. TABLE 2.1 tabulates their nomenclature and provides brief comments. The energy position of the luminescence lines and bands may depend on strain in thin GaN layers, temperature, and excitation intensity. Therefore, in TABLE 2.1 the energy positions corresponding to the strain-free GaN at low temperatures are given.

26

iii. Cathodoluminescence (CL)

Cathodoluminescence is an optical and electrical phenomenon whereby a beam of electrons is generated by an electron gun (e.g., cathode ray tube) and then impacts on a luminescent material such as a phosphor, causing the material to emit visible light. The most common example is the screen of a television. In geology, mineralogy and materials science a scanning electron microscope with specialized optical detectors, or an optical cathodo-luminescence microscope, is used to examine internal structures of semiconductors, rocks, ceramics, glass, etc. in order to get information on the composition, growth and quality of the material.

Cathodoluminescence occurs because the impingement of a high energy electron beam onto a semiconductor will result in the promotion of electrons from the valence band into the conduction band, leaving behind a hole. When an electron and a hole recombine, it is possible for a photon to be emitted. The energy of the photon, and the probability that a photon and not a phonon will be emitted, depends on the material, its purity, and its defect state.

In this case, the "semiconductor" examined can, in fact, be almost any non-metallic material. In terms of band structure, classical semiconductors, insulators, ceramics, gemstones, minerals, and glasses can be treated the same way.

27

TEBLE 2.1 List of main luminescence lines and bands in GaN. [1]

Maximum Position (eV)	Nomenclature	Doping	Comments
3.478	FE, X_A	Undoped	
3.471	DBE, D^oX_A	Undoped, Si	A few close lines
3.466	ABE, A^oX_A	Undoped, Mg	Best FWHM <0.1 meV
3.44-3.46	TES	Undoped	Plethora of lines
3.455	ABE	Zn	A weaker peak at 3.39 eV
3.45-3.46	Y_1	Undoped	Correlates with inversion domains
3.41-3.42	Y_2	Undoped	
3.397		Be	e-A type
3.387	FE-LO	Undoped	
3.38	DBE-LO	Undoped	
3.38		Be	DAP type
3.37-3.38	Y_3		Undoped
3.375	ABE-LO	Undoped	
3.364	ABE-LO	Zn	
3.35-3.36	Y_4	Undoped	
3.34	Y_5	Undoped	
3.30-3.32	Y_6	Undoped	
3.295	FE-2LO	Undoped	
3.288	DBE-2LO	Undoped	
3.283	ABE-2LO	Undoped	
3.28	UVL	Undoped	e-A type
3.272	ABE-2LO	Zn	
3.27	DBE		DBE in cubic GaN
3.26	UVL	Undoped, Si	DAP type
3.1-3.26	UVL	Mg	e-A and DAP
3.21-3.23	Y_7	Undoped	
3.16			Shallow DAP in cubic GaN
3.08	Y_8	Undoped	
3.08		C	In cubic GaN
3.0-3.05	BL	C	Broad

28

In materials science and semiconductor engineering, cathodoluminescence will mostly be performed in either a scanning electron microscope or a scanning transmission electron microscope. In these cases, the highly focused beam of electrons impinges on a sample and induces it to emit light from a localized area. This light will be collected by an optical system, such as an elliptical mirror. From there, a fiber optic will transfer the light out of the microscope where it will be separated by a monochromator and then detected with a photomultiplier tube. By scanning the microscope's beam in an X-Y pattern and measuring the light emitted with the beam at each point, a map of the optical activity of the specimen can be obtained. The primary advantages to the electron microscope based technique is the ability to resolve features down to 1 nano-meter [2], the ability to measure an entire spectrum at each point (hyperspectral imaging) if the photomultiplier tube is replaced with a CCD camera, and the ability to perform nanosecond- to picosecond-level time-resolved measurements if the electron beam can be "chopped" into nano- or pico-second pulses. Moreover, the optical properties of an object can be correlated to structural properties observed with the electron microscope. These advanced techniques are useful for examining low-dimensional semiconductor structures, such a quantum wells or quantum dots. However, as the abilities are improved, the cost of the electron-microscope based techniques becomes very high.

Although direct bandgap semiconductors such as GaAs or GaN are most easily examined by these techniques, indirect semiconductors such as silicon also emit weak levels of light, and can be examined as well. In particular, the luminescence of

29

dislocated silicon is different from intrinsic silicon, and can be used to map defects in integrated circuits.

Except of the much higher magnification and good versatility, an electron microscope with a cathodoluminescence detector will be more complicated and more expensive compared to an easy to use optical cathodoluminescence microscope which benefits from its ability to show actual visible color features immediately through the eyepiece.

In short, cathodoluminescence is a technique that can be implemented in an optical or electron microscope with the proper accessories, and allows the optical properties of non-metallic materials to be examined.

iv. Transmission electron microscopy (TEM)

Transmission electron microscopy (TEM) has, in four decades time, become a mainstay in the repertoire of characterization techniques for materials science. Strong advantages of TEM are its high lateral spatial resolution (about 0.1 nm point-to-point resolution on some instruments) and its capability to provide both image and diffraction information from a single sample. In addition, the highly energetic beam of electrons (enable to a nanometer scale proving) used in TEM interacts with sample matter to produce characteristic radiation and particles; these signals often are measured to provide materials characterization using x-ray dispersive spectroscopy (XDS), electron energy loss spectroscopy (EELS), back scattered and

secondary electron imaging, to name a few possible technique. In TEM, a focused electron beam is incident on a thin (nominally less than 200 nm) sample. The signal in TEM is obtained from both undeflected and deflected electrons that penetrate the sample thickness. Fig. 2. 4 shows the schematic illustration of TEM geometry. Magnetic lenses below the sample position are responsible for delivering the signal to detectors such as a fluorescent screen, a film plate, or video camera. Accompanying this signal information is a magnification of the special information in the signal by as little as 50 times to as much as a factor of 106. This remarkable magnification range is facilitated by the small wavelength of the incident electrons, and is the key to unique capabilities associated with TEM analysis.
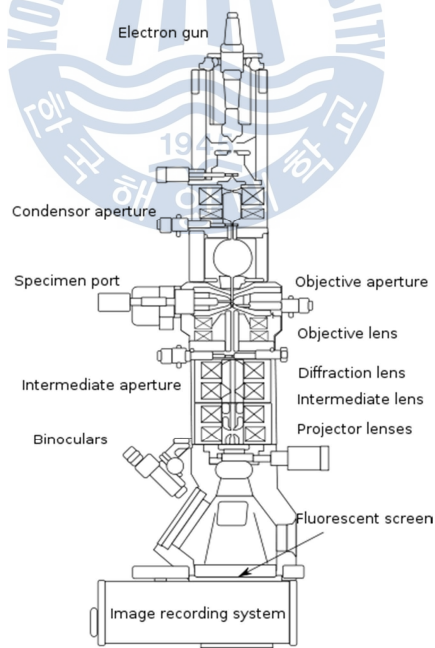
Fig. 2.4 Schematic diagram of TEM system

v. x-ray diffraction (XRD)

X-ray diffraction (XRD) is a method for non-destructive ex-situ investigation of thin films. The information concerning the composition and uniformity of epitaxial layers, thickness, built-in stress and its relaxation, and the crystalline perfection can be obtained. Fig. 2.5 shows the schematic illustration of HR-XRD geometry. It consists of a monochromator, a multiple reflection analyzer crystal for high intensity and resolution measurement for reciprocal lattice scans.
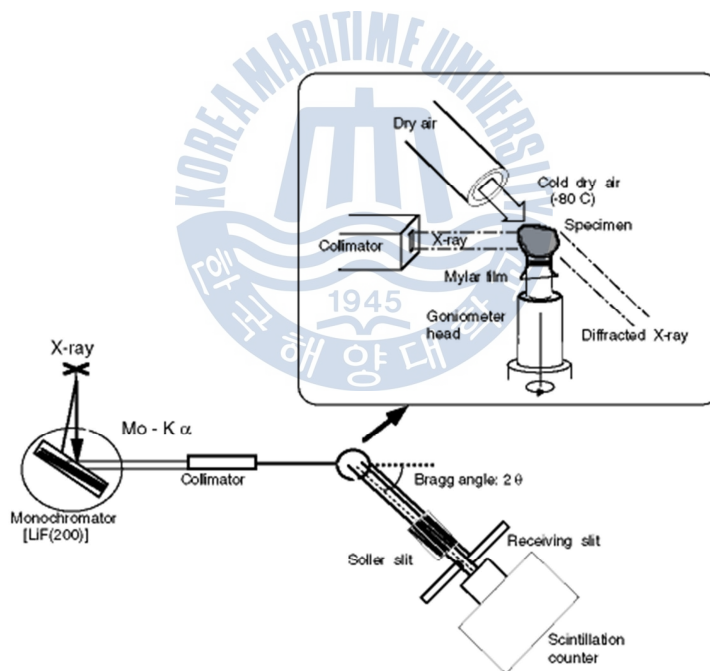
Fig. 2.5 Schematic of the system for the X-ray diffraction measurement

For a beam source of X-ray Cu-Kα1 (wavelength =1.54060Å) radiation was used, and diffraction occurs satisfying Bragg's law. The Kα2component is suppressed to a level below 0.1%.

In this study, two kinds of scan method were mainly used. One is the most widely used X-ray characterization method, ω-2θ scan, and another is a rocking curve scan, ω-scan, for characterizing the mosaicity in a crystal. One can get information on growth direction, crystal structure, and lattice constant using the ω-2θ scan and crystallinity concerned on tilt or twist angles using the rocking curve scan.

B. Theoretical Background : Defects in GaN crystal

Point defects

Point defects are defects that occur only at or around a single lattice point. They are not extended in space in any dimension. Strict limits for how small a point defect is, are generally not defined explicitly, but typically these defects involve at most a few extra or missing atoms. Larger defects in an ordered structure are usually considered dislocation loops. For historical reasons, many point defects, especially in ionic crystals, are called centers: for example a vacancy in many ionic solids is called a luminescence center, a color center, or F-center. These dislocations permit ionic transport through crystals leading to electrochemical reactions. These are frequently specified using Kröger–Vink Notation.

33
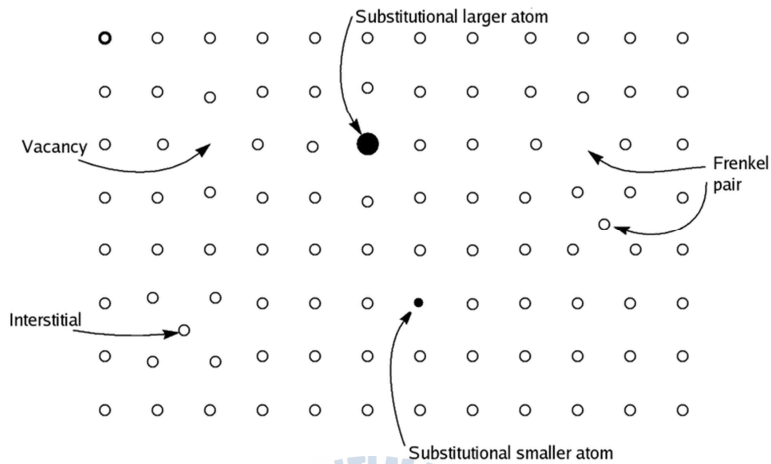
Fig. 2.6 Schematic illustration of some simple point defect types in a monatomic

solid

Vacancy defects are lattice sites which would be occupied in a perfect crystal, but are vacant. If a neighboring atom moves to occupy the vacant site, the vacancy moves in the opposite direction to the site which used to be occupied by the moving atom. The stability of the surrounding crystal structure guarantees that the neighboring atoms will not simply collapse around the vacancy. In some materials, neighboring atoms actually move away from a vacancy, because they experience attraction from atoms in the surroundings. A vacancy (or pair of vacancies in an ionic solid) is sometimes called a Schottky defect.

Interstitial defects are atoms that occupy a site in the crystal structure at which

34

there is usually not an atom. They are generally high energy configurations. Small atoms in some crystals can occupy interstices without high energy, such as hydrogen in palladium.

A nearby pair of a vacancy and an interstitial is often called a Frenkel defect or Frenkel pair. This is caused when an ion moves into an interstitial site and creates a vacancy.

Impurities occur because materials are never 100% pure. In the case of an impurity, the atom is often incorporated at a regular atomic site in the crystal structure. This is neither a vacant site nor is the atom on an interstitial site and it is called a substitutional defect. The atom is not supposed to be anywhere in the crystal, and is thus an impurity. There are two different types of substitutional defects, Isovalent substitution and aliovalent substitution. Isovalent substitution is where the ion is substituting the original ion of the same oxidation state as the ion is replacing. Aliovalent substitution is where the ion is substituting the original ion of a different oxidation state as the ion is replacing. Aliovalent substitutions change the overall charge within the ionic compound, but the ionic compound must be neutral. Therefore a charge compensation mechanism is required. Hence either one of the metals is partially or fully oxidised or reduced, or ion vacancies are created.

Antisite defects [3-4] occur in an ordered alloy or compound when atoms of different type exchange positions. For example, some alloys have a regular structure in which every other atom is a different species; for illustration assume that type A

35

atoms sit on the corners of a cubic lattice, and type B atoms sit in the center of the cubes. If one cube has an A atom at its center, the atom is on a site usually occupied by a B atom, and is thus an antisite defect. This is neither a vacancy nor an interstitial, nor an impurity.

Topological defects are regions in a crystal where the normal chemical bonding environment is topologically different from the surroundings. For instance, in a perfect sheet of graphite (graphene) all atoms are in rings containing six atoms. If the sheet contains regions where the number of atoms in a ring is different from six, while the total number of atoms remains the same, a topological defect has formed. An example is the Stone Wales defect in nanotubes, which consists of two adjacent 5-membered and two 7-membered atom rings.

Also amorphous solids may contain defects. These are naturally somewhat hard to define, but sometimes their nature can be quite easily understood. For instance, in ideally bonded amorphous silica all Si atoms have 4 bonds to O atoms and all O atoms have 2 bonds to Si atom. Thus e.g. an O atom with only one Si bond (a dangling bond) can be considered a defect in silica [5].

Complexes can form between different kinds of point defects. For example, if a vacancy encounters an impurity, the two may bind together if the impurity is too large for the lattice. Interstitials can form 'split interstitial' or 'dumbbell' structures where two atoms effectively share an atomic site, resulting in neither atom actually occupying the site.

Dislocation

In materials science, a dislocation is a crystallographic defect, or irregularity, within a crystal structure. The presence of dislocations strongly influences many of the properties of materials. The theory was originally developed by Vito Volterra in 1905 but the term 'dislocation' was not coined until later by the late Professor Sir Frederick Charles Frank of the Physics Department at the University of Bristol. Some types of dislocations can be visualized as being caused by the termination of a plane of atoms in the middle of a crystal. In such a case, the surrounding planes are not straight, but instead bend around the edge of the terminating plane so that the crystal structure is perfectly ordered on either side. The analogy with a stack of paper is apt: if a half a piece of paper is inserted in a stack of paper, the defect in the stack is only noticeable at the edge of the half sheet.

There are two primary types: edge dislocations and screw dislocations. Mixed dislocations are intermediate between these.

Mathematically, dislocations are a type of topological defect, sometimes called a soliton. The mathematical theory explains why dislocations behave as stable particles: they can be moved about, but maintain their identity as they move. Two dislocations of opposite orientation, when brought together, can cancel each other (this is the process of annihilation), but a single dislocation typically cannot "disappear" on its own.

Edge dislocations

An edge dislocation is a defect where an extra half-plane of atoms is introduced mid way through the crystal, distorting nearby planes of atoms. When enough force is applied from one side of the crystal structure, this extra plane passes through planes of atoms breaking and joining bonds with them until it reaches the grain boundary. A simple schematic diagram of such atomic planes can be used to illustrate lattice defects such as dislocations. (Fig. 2. 7   represents the "extra half-plane" concept of an edge type dislocation). The dislocation has two properties, a line direction, which is the direction running along the bottom of the extra half plane, and the Burgers vector which describes the magnitude and direction of distortion to the lattice. In an edge dislocation, the Burgers vector is perpendicular to the line direction.
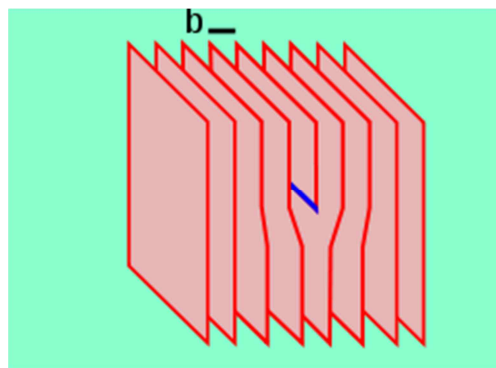
Fig. 2.7 Schematic diagram (lattice planes) showing an edge dislocation. Burgers vector in black, dislocation line in blue.

The stresses caused by an edge dislocation are complex due to its inherent asymmetry.

These stresses are described by three equations: [6]

$$\sigma_{xx} = \frac{-\mu b}{2\pi(1-\nu)} \frac{y(3x^2 + y^2)}{(x^2 + y^2)^2}$$

$$\sigma_{yy} = \frac{-\mu b}{2\pi(1-\nu)} \frac{y(x^2 - y^2)}{(x^2 + y^2)^2}$$

$$\tau_{xy} = \frac{-\mu b}{2\pi(1-\nu)} \frac{x(x^2 - y^2)}{(x^2 + y^2)^2}$$

where μ is the shear modulus of the material, b is the Burgers vector, ν is Poisson's ratio and x and y are coordinates.

These equations suggest a vertically oriented dumbbell of stresses surrounding the dislocation, with compression experienced by the atoms near the "extra" plane, and tension experienced by those atoms near the "missing" plane.[6]

Screw dislocations

A screw dislocation is much harder to visualize. Imagine cutting a crystal along a plane and slipping one half across the other by a lattice vector, the halves fitting back together without leaving a defect. If the cut only goes part way through the crystal, and then slipped, the boundary of the cut is a screw dislocation. It comprises

Collection

a structure in which a helical path is traced around the linear defect (dislocation line) by the atomic planes in the crystal lattice (Fig. 2. 8). Perhaps the closest analogy is a spiral-sliced ham. In pure screw dislocations, the Burgers vector is parallel to the line direction.
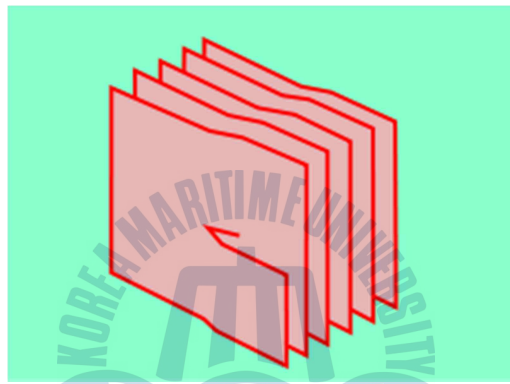
Fig. 2.8 Schematic diagram (lattice planes) showing a screw dislocation.

Despite the difficulty in visualization, the stresses caused by a screw dislocation are less complex than those of an edge dislocation. These stresses need only one equation, as symmetry allows only one radial coordinate to be used:[6]

$$\tau_r = \frac{-\mu b}{2\pi r}$$

where μ is the shear modulus of the material, b is the Burgers vector, and r is a radial coordinate. This equation suggests a long cylinder of stress radiating outward from the cylinder and decreasing with distance. Please note, this simple model

40

results in an infinite value for the core of the dislocation at r=0 and so it is only valid for stresses outside of the core of the dislocation.[6]

Mixed dislocations

In many materials, dislocations are found where the line direction and Burgers vector are neither perpendicular nor parallel and these dislocations are called mixed dislocations, consisting of both screw and edge character.

Stacking Faults

Stacking faults occur in a number of crystal structures, but the common example is in close-packed structures. Face-centered cubic (fcc) structures differ from hexagonal close packed (hcp) structures only in stacking order: both structures have close packed atomic planes with six fold symmetry—the atoms form equilateral triangles. When stacking one of these layers on top of another, the atoms are not directly on top of one another—the first two layers are identical for hcp and fcc, and labelled AB. If the third layer is placed so that its atoms are directly above those of the first layer, the stacking will be ABA—this is the hcp structure, and it continues ABABABAB. However, there is another possible location for the third layer, such that its atoms are not above the first layer. Instead, it is the atoms in the fourth layer that are directly above the first layer. This produces the stacking ABCABCABC,

41

and is actually a cubic arrangement of the atoms. A stacking fault is a one or two layer interruption in the stacking sequence, for example, if the sequence ABCABABCAB were found in an fcc structure.
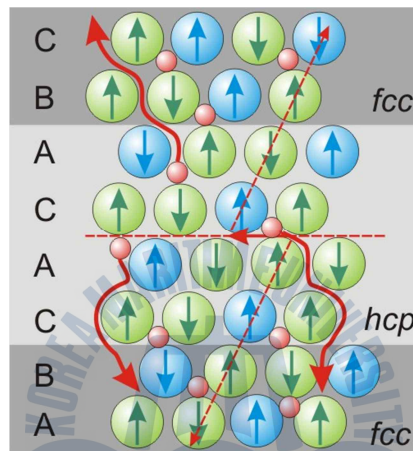
Fig. 2.9 Sketch of the stacking fault in fcc structure

References

[1] M. A. Reshchikov and H. Morkoc, J. Appl. Phys. 97 (2005) 061301.

[2] L. Fernando Zagonel, S. Mazzucco, M. Tence, K. March, R. Bernard, B. Laslier, G. Jacopin, M. Tchernycheva, L. Rigutti, F. H. Julien, R. Songmuang and M. Kociak, Nano Lett. 11 (2011), 568.

[3] T. Mattila, R. M. Nieminen, Phys, Rev. Lett. 74 (1995) 2721.

[4] H. Hausmann, A. Pillukat, P. Ehrhart, Phys, Rev. Lett. B 54 (1996)

[5] K.-P. Lieb, J. Keinonet, Cotem. Phys. 47 (2006) 305

[6] R. E. Reed-Hill, (1994) "Physical Metallurgy Principles"

Chapter 3. HVPE Growth of reduced defect density polar GaN

3-1. Introduction

It is well-known that difficulty of making GaN substrate hinders a development of high performance devices like as vertical current injection light emitting diode (LED). Hence, the significance of high quality pseudo-GaN substrate is becoming more important. Hydride vapor phase epitxy (HVPE) is very suitable method to obtain thick GaN for substrate due to its high growth rate. This fact made many research groups study various ways of growing low defect density and crack free GaN by HVPE [1,2]. Another pending issue is the separation of sapphire substrate from GaN thick layer, because substrate separation is a rigorous and time-consuming processes [3]. Recently, one of the authors of this paper reported on the HVPE-GaN by using a $GaCl_3$ buffer layer. The buffer layer was named as an evaporable-buffer-layer (EBL) [4], which was designed to separate the substrate easily without any help of additional processes. However, the rapid improvement of crystal quality is very essential for this technique, since this method is basically an overgrowth technique by using polycrystalline crystallites (GaN) in the amorphous layer ($GaCl_3$).

This chapter has proposed the insertion of GaN layer grown at an intermediate temperature (IT-GaN; $T_g = 900^{\circ}C$). It is very simple method due to just modification

of the normal HVPE procedure and it improve the crystalline of GaN layer remarkably with reduced threading dislocation [5]. The effect of IT-GaN on overgrown GaN crystalline was demonstrated by comparing with GaN film without IT-GaN

3-2. Experimental details

AlN templates grown on (0001) Al_2O_3 substrates were prepared by metal organic chemical vapor deposition (MOCVD). Trimethylaluminum (TMA) and ammonia (NH_3) were used as Al and N sources, respectively. The substrate temperature was ~1080°C for AlN films. Subsequently, two GaN samples are prepared: one was a GaN film without an IT-GaN (Sample A), and the other was a GaN film grown on an IT-GaN (Sample B). The GaN films were grown on AlN/sapphire templates by hydride vapor phase epitaxy (HVPE). The growth began with a nitridation process using an AlN/sapphire template for 30 min at 1080°C; subsequently, thick GaN films were grown at 1040℃ and IT-GaN grown on the template at 900°C.

The surface morphology was analyzed using atomic force microscopy (AFM). An x-ray diffraction (XRD) measurement was performed to confirm the crystal quality and residual strain of the films. To characterize the optical properties, low-temperature (11K) photoluminescence (PL) was measured using the 325 nm line of a He-Cd laser as an excitation light source. Also cross-sectional CL and TEM were

45

used to analyze the depth profile of TDs in Sample B. For the cross-sectional CL measurement, ion milling was applied to diminish the artifact due to rough surface.

3-3. Surface morphology

Fig. 3.1 shows the AFM images of Samples A (Fig. 3.1(a)) and B (Fig. 3.1(b)). As shown in Fig. 3.1(b), Sample B had a smoother surface than Sample A.
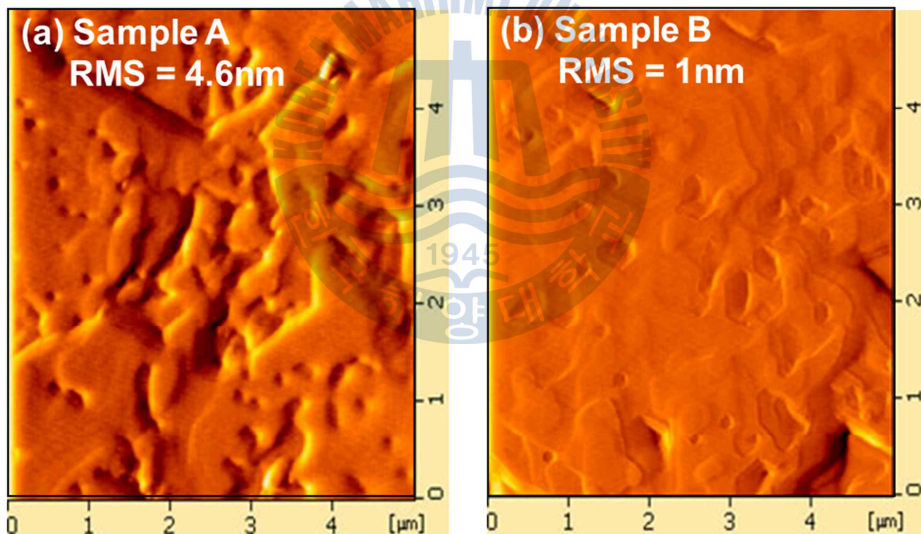
Fig. 3.1 AFM images of GaN samples: (a) Sample A, and (b) Sample B

The root-mean square (RMS) roughness values for the samples were notably different; Sample A showed a relatively rough (4.6 nm) surface, but Sample B showed a smooth surface (1.0 nm). The lattice defects are known to have a strong

relationship with surface morphology and with the strain of the film [6]. Hence, the results shown in Fig. 3.1 imply a considerable difference in the structural quality of the two samples.

3-4. Evaluation by XRD

Fig. 3.2 shows the XRD rocking curves for GaN symmetric (002) and asymmetric (102) reflections. Sample A (Fig. 3.2a) showed an FWHM of 231 and 249 arcseconds for (002) and (102) reflections, respectively. Sample B (Fig. 3.2b), however, showed an XRC FWHM of 128 and 1239 arcseconds for (002) and (102) reflections, respectively. It is well known that the FWHM of an X-ray rocking curve includes various information such as crystal size effect, local strain and defect density in the film. When a film has a thickness of a few tenths of a μm, one can neglect the crystal size effect and assume that the XRC broadening is caused by crystal defects in the film.
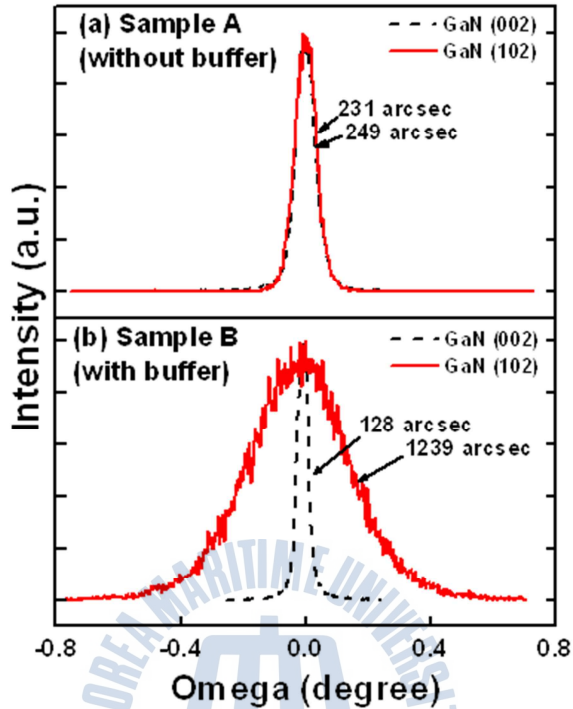
Fig. 3.2 X-ray rocking curves (ω-scans) of HVPE-GaN films: (a) Sample A,
and (b) Sample B.

The dislocation densities of Samples A and B were evaluated using the FWHM values of XRC. The screw- and edge-dislocation densities (N_{screw} and N_{edge}, respectively) were calculated using the following formulas [7,8]:

$$N_{screw} = \alpha_{tilt}^2/4.35b_c^2 \quad (1)$$

$$N_{edge} = \alpha_{twist}^2/4.35b_a^2 \quad (2)$$

Where b_c and b_a are the Burgers vectors of the c-type and a-type dislocations,

48

respectively ($|b_c| = c = 0.5185nm$, and $|b_a| = a = 0.3189nm$ [8]), and α_{tilt} and α_{twist} represent the tilt and twist angles. For Sample A, the respective screw- and edge-dislocation densities were evaluated to be 1.07×10^8 cm^{-2} and 3.29×10^8 cm^{-2}, while a relatively low screw-dislocation density (3.29×10^7 cm^{-2}) and a high edge-dislocation (8.15×10^9 cm^{-2}) density were obtained for Sample B. Those dislocation density values are comparable to the reported values when the thickness of the samples [9] is considered. The screw-dislocation density of Sample B was reduced to 0.3 times that of Sample A, but the edge-dislocation density of Sample B was ~25 times higher that of sample A. This result revealed that the dislocation generated during the growth of the IT-buffer was mainly an edge component.
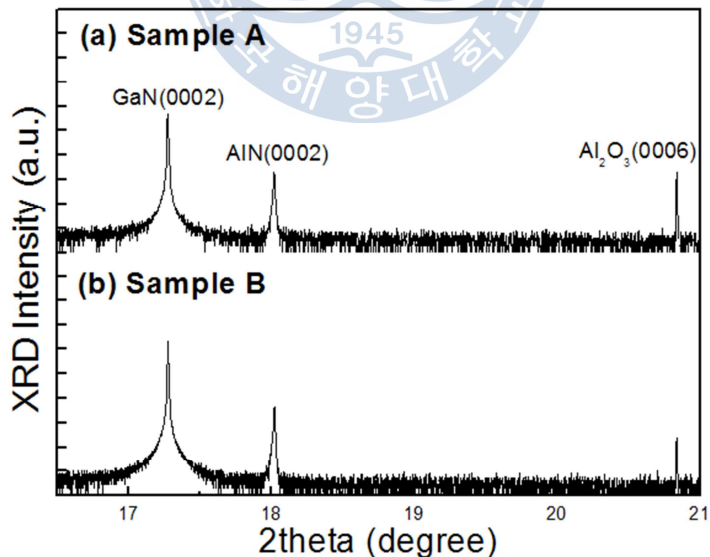
Fig. 3.3 X-ray diffractions (ω-2θ scan) for the HVPE-GaN films: (a) Sample A, and (b) Sample B

49

Fig. 3.3 shows the XRD ω-2θ scan of Samples A and B. The strains were evaluated [10] as a 0.3% compressive strain for Sample A and an 0.08% tensile strain for Sample B regardless of identical thicknesses. The residual strain and defect density in a film can be simply discussed from a thermodynamical viewpoint. The Gibbs free energy of a film includes the interface, the surface, and the internal energy of a film. When the interfacial and surface energy is identical, a different residual strain equates to a different internal energy for a film. Because two samples were prepared with an identical interface structure ($GaN/AlN/Al_2O_3$), the interface energy was regarded as identical. Thus, the difference in the Gibbs free energies of the two samples may have resulted from the surface or internal energies. Actually, the surface and internal energies of a film are closely related. In a heteroepitaxy, a misfit relaxation will accommodate residual strain and reduce the internal energy of the film. Also, minimization of the internal energy of a film is necessary to obtain a smooth surface. Therefore, the smooth surface (Fig. 3.1(b)) and low residual strain (Fig. 3.3(b)) of Sample B (in comparison with Sample A) is understandable due to the high edge-dislocation density (Fig. 3.2(b)) of the sample.

However, it is worth noting that, generally, a high accommodation rate equates to poor crystal quality because dislocations will only be terminated at the film surface. Therefore, several techniques, such as multiple buffer layers [11] or annealing at a high temperature [12], have been introduced to improve the crystallinity of highly relaxed film by terminating dislocation propagation. This description raises questions concerning the position of edge dislocations. In the case

50

of Sample B, if the reduction of the residual strain in the HT-GaN layer is achieved by allowing the generation of high-density dislocations in the HT-GaN layer, the IT-GaN growth should be avoided. Hence, crystallinity of the HT-GaN layer should be compared to estimate the threading-dislocation density in that region. Photoluminescence (PL) is a suitable method for this purpose, because it contains information within an absorption depth of excitation light.

3-5. Low temperature PL spectrum
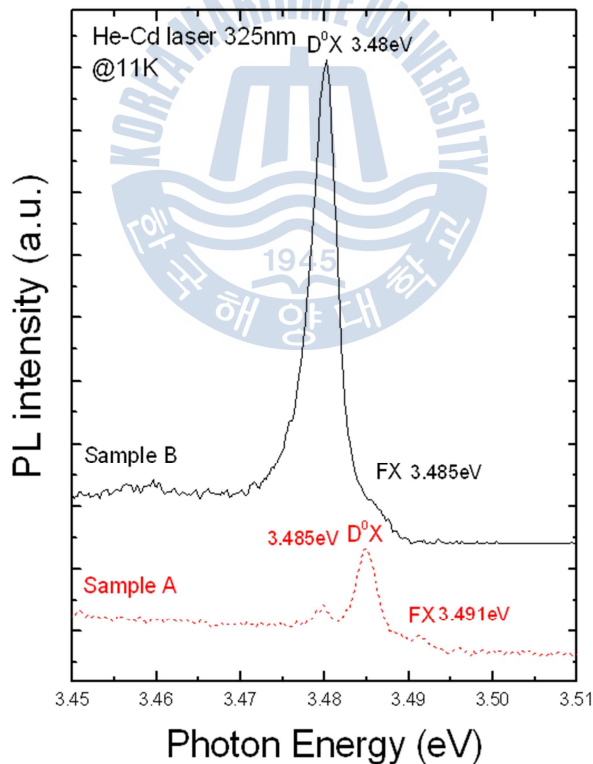
Fig. 3.4 Low-temperature PL spectra of the HVPE-GaN films:(a) Sample A, and (b) Sample B.

Fig. 3.4 shows the low temperature PL spectra of both samples at 11K. Sample B showed remarkably strong luminescence intensity and a narrow PL FWHM in comparison with Sample A. These results clearly show that optical properties were improved by inserting the IT-GaN. Hence, It was attributed that the dislocations mainly to inclusion of the IT-GaN. This could have been caused by either the generation of edge-type dislocations during the IT-GaN growth or by the terminating of screw-type dislocations. The latter can be achieved by an unwilling terminating process during the HVPE. However, no dislocation-terminating processes was adopted, and Sample B had two interfaces (one was IT-GaN/AlN and the other was HT-GaN/IT-GaN) and HVPE growth was interrupted just after finishing the IT-GaN growth to increase the growth temperature for HT-GaN. Therefore, it was concluded that the IT-GaN accommodated misfit by generating an edge-type dislocation and terminating screw-type dislocation at the IT/HT-GaN interface, however, the mechanism of the edge-type dislocation generation during the growth of the IT-GaN should be studied further.

And then CL and TEM measurement of Sample B was performed to study reason of TD reduction by the IT-GaN layer.

3-6. CL image and spectrum

Fig. 3.5 (a) shows the cross-sectional CL image of the HVPE GaN. This image reveals well the columnar structure of GaN. Generally dislocations make dark

52

contrast in the CL images, since they act as a non-radiative recombination center [13]. Therefore, we tentatively assigned the vertical dark lines to TDs in GaN. The dislocation density of P1 in the IT-GaN near the AlN/IT-GaN interface is as high as 1.2×10^8 cm^{-2}. While it decreases to 6.7×10^7 cm^{-2} at P2 near the IT-GaN/high temperature GaN (HT-GaN) interface. Also, it decreases further to 9.2×10^6 cm^{-2} at P3 in HT-GaN film.
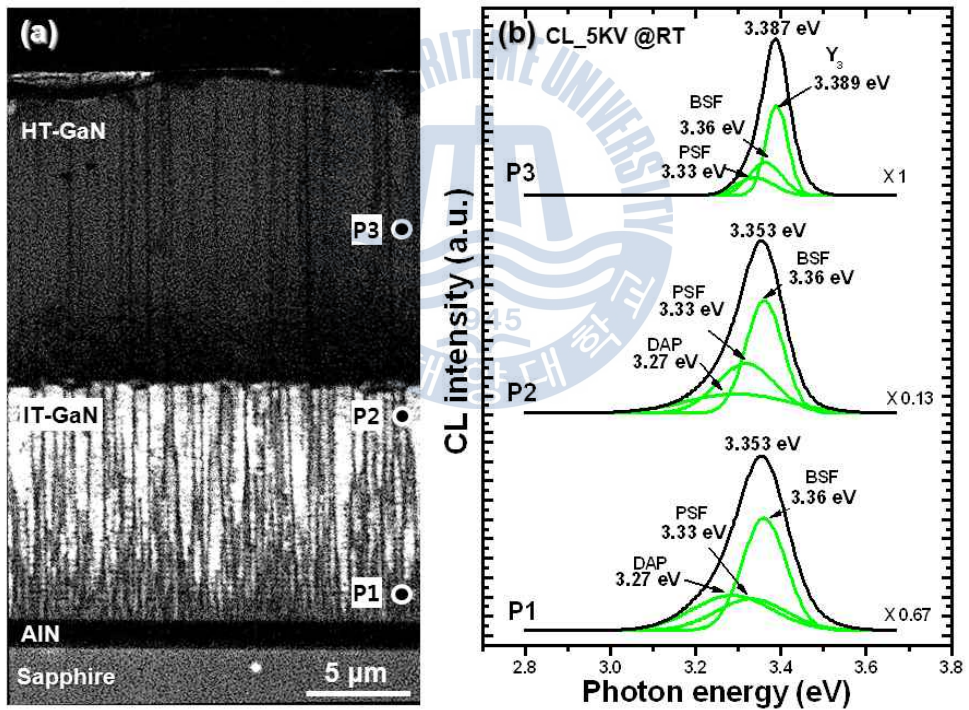
Fig. 3.5 (a) Cross-sectional CL image of the GaN film with IT-GaN (Sample B). (b) CL spectra of the GaN/IT-GaN observed at each points P1, P2 and P3 in the Fig. 3. 5 (a).

It is worthy to noting that, in the Fig. 3. 5(a), the IT-GaN region is looking relatively brighter than the overgrown HT-GaN layer. The IT-GaN might contain high density defects due to the low growth temperature. It indicates that the IT-GaN contains high density defect which acts as an efficient luminescence center in the GaN. The most presumable structural imperfection is the stacking faults (SF). The formation every per unit cell area of four different types SFs in GaN were reported as 10 meV for type-I, 24 meV for type-II, 19 meV for type-III, and 38 meV for extrinsic SFs [14]. Type-I SF of GaN has the lowest formation energy among the all SFs in GaN, AlN, and InN. Also, SFs in GaN have been known as an active luminescence center [15] by the collaboration of TEM and CL observations. Hence, if the IT-GaN contains high density SFs, bright CL image could be observed as reported before [14]. Therefore, we attributed the bright CL image to the SF in GaN. Consequently, the Fig. 1(a) can be understood as follows; 1) high density SFs were generated in the IT-GaN, 2) the TD density gradually reduced during the growth of IT-GaN.

For more discussion, CL spectra were observed along with the growth direction. Fig. 1(b) shows the CL spectra measured at the points of P1, P2 and P3. Broad and asymmetric luminescence bands were observed from all points. As shown in the Fig. 1(b), we decomposed the broad emission line by using four peaks centered at 3.27 eV, 3.33 eV, 3.36 eV and 3.39 eV. Those peaks are well known as donor-acceptor pair (DAP, 3.27eV) [16], prismatic stacking fault (PSF, 3.33 eV) [17], basal stacking fault (BSF, 3.36 eV) [18] and Y3 (3.39 eV) [16] related dislocations. Note that it is

quite different from the PL spectrum obtained from the surface. From the PL spectrum taken at the surface, we could observe a strong luminescence from DX emission at 3.42 eV [12], which is remarkably different from the cross-sectional CL spectra in the Fig.3.5 (b). This fact indicates well that the CL spectra reflect well the structural defects profile along with the growth direction. The CL spectra of P1 and P2 revealed basically the same spectrum which could be decomposed by mainly SF and impurity related emissions. However, CL spectra of P3 clearly shows reduced participation of SF related emission lines and increase of near band edge emission intensity, although the overall luminescence intensity itself is weaker than CL spectra of both P1 and P2. Those CL spectra correspond well with our explanation about the CL image. However, we need TEM observation to confirm it.

3-7. TEM measurement

Fig. 3.6 shows cross-sectional TEM micrograph of HVPE GaN, which is piled up of local images from substrate to HT-GaN. It shows basically the same result as the CL image in Fig. 3.5 (a). We could observe a high density TD lines at the AlN/IT-GaN interface. However, HT-GaN contains a low TD density.

Fig. 3.6 Piled cross-sectional TEM micrograph for GaN film with IT-GaN (Sample

B)

Fig. 3.7 shows a distribution of edge (Fig. 3.7 (a) and (b)) and screw (Fig. 3.7(c) and (d)) component of dislocations in the HVPE GaN Fig. 3.7 (a) and (b) are the TEM images with g=<1-100> , while Fig. 3.7 (c) and (d) are TEM images with g=<0002>.
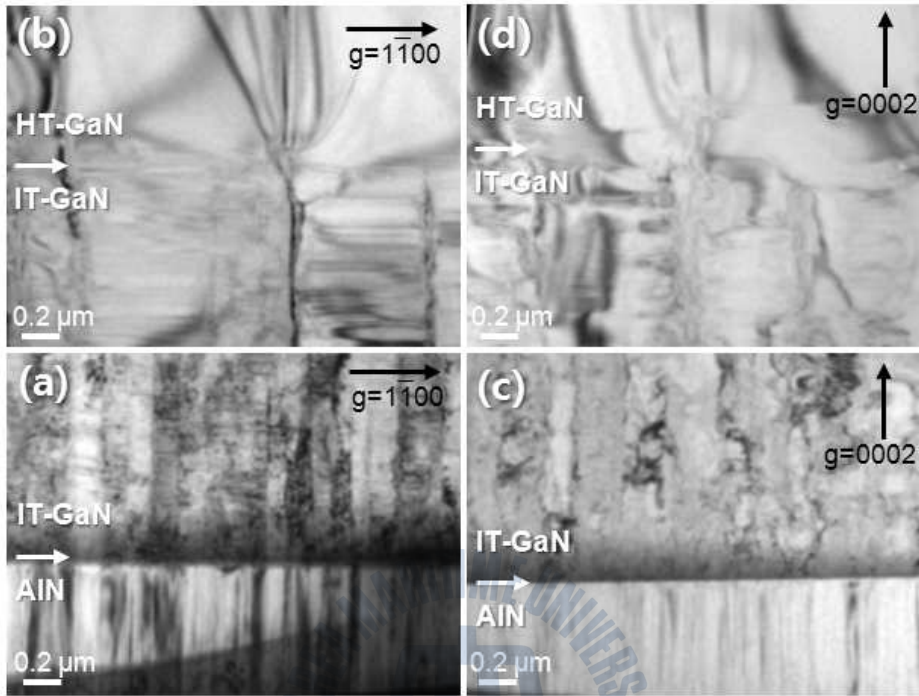
Fig. 3.7 Cross-sectional TEM micrographs take under the two-beam conditions at the HT-GaN/IT-GaN and IT-GaN/AlN interfaces. The images (a) and (b) were obtained with g=1-100 condition, while (c) and (d) were obtained with g=0002 condition.

In the Fig. 3.7 (a), AlN layer has a high edge dislocation (ED) density of 6.4×10^9 cm^{-2} , while IT-GaN has an ED density of 3.4×10^9 cm^{-2} and high density SFs are observed in the IT-GaN. Fig. 3.7 (b) is the TEM image near the HT-GaN/IT-GaN interface. IT-GaN has an ED density of 6×10^8 cm^{-2} and high density SFs. While HT-GaN has an ED density of 4.5×10^8 cm^{-2} without SF. On the other hand, Fig. 3.7 (c) shows that the screw dislocation (SD) densities of AlN and IT-GaN are

57

4×10^9 cm^{-2} and 2.3×10^8 cm^{-2}, respectively. Also, we could find out from the Fig. 3.7 (d) that during the IT-GaN growth, the SD density decreased 9.3×10^7 cm^{-2} and it decreased further to 5.4×10^7 cm^{-2} for HT-GaN. TD density evolution is summarized in the Table 1. In the CL measurement, TD density decreased from 1.2×10^8 cm^{-2} to 9.2×10^6 cm^{-2}. While the SD density observed by TEM changed from 2.3×10^8 cm^{-2} to 5.4×10^7 cm^{-2}, and in case of ED density 6×10^8 cm^{-2} to 4.5×10^8 cm^{-2} at the same region. The discrepancy between CL and TEM evaluation results of dislocation density is unclear. However, remind that CL image is based on the luminescence, while TEM image is based on the diffraction, hence spatial resolutions of two methods should be different.

TABLE 3.1 Evolution of threading dislocation density (NA;not available)

Positions		Dislocation density (cm^{-2})		
		TEM		CL
		g = 1-100	g= 0002	
HT-GaN		4.5×10^8	5.4×10^7	9.2×10^6
IT-GaN	HT-GaN/IT-GaN	6×10^8	9.3×10^7	6.7×10^7
	IT-GaN/AlN	3.4×10^9	2.3×10^8	1.2×10^8
AlN		6.4×10^9	4×10^9	NA

Fig. 3.8 shows threading dislocation densities with increasing film thickness. The solid line is a calculated result based on the crystal size effect [19], which can be understood as the ideal crystal quality of GaN film along with the thickness, since it was calculated from the XRD linewidth broadening from a perfect crystal just depends on the thickness of a film.
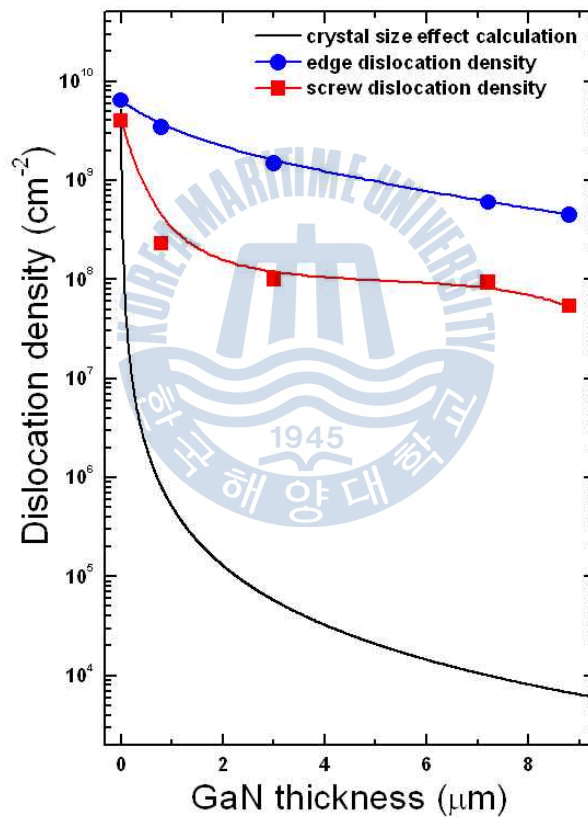

Fig. 3.8 Dislocation density variation along with the film thickness. The solid line is the calculated result from the crystal size effect. Circles and squares are indicating edge and screw dislocations, respectively.

Fig. 3.8 showed well that the reduction of ED density is very difficult similar to many other reports. The ED density reduced gradually along with the film growth. While, fast SD density reduction have achieved from the very initial stage of IT-GaN growth. Also, as one can observe, the SD density reduced faster during the growth of IT-GaN than HT-GaN. When we define the dislocation reduction rate (r_{dr}) as the reduced dislocation density (D_d) per unit thickness; $r_{dr}=\Delta D_d/thickness(\mu m)$, in case of SD, r_{dr} was as high as $1.59 \times 10^7 cm^{-2}/\mu m$ for the IT-GaN, but it decreased to $0.45 \times 10^7 cm^{-2}/\mu m$. For the ED, r_{dr} was as low as $0.33 \times 10^7 cm^{-2}/\mu m$ for the IT-GaN, but it further decreased to $0.017 \times 10^7 cm^{-2}/\mu m$. Reduction of TD can be achieved through various paths such as bending at the surface, merging with the other one, and interacting with other defects. Also all those factors are closely related with the crystal structure of the material. Bending can be excluded in this discussion, because the IT-GaN does not contain any interface. Merging can be enhanced when the TD density is high. But generally dislocation reduction by merging would be enhanced by the two-dimensional growth under the high growth temperature. Hence, it could not play the dominant role for the reduction of dislocation density in the IT-GaN. Finally, interacting with other defects will also be enhanced when the film contains high density structural defects. It was founded that IT-GaN contains high density SFs due to its low growth temperature. Therefore, interaction between TDs and SFs should be considered as a main TD reduction mechanism. Most common stacking faults in wurtzite GaN have the following stacking sequences [20] αbβ<u>aαbβcγ</u>bβcγ (I_1) and the corresponding Burgers vector of surrounding partial dislocations is b=1/6 [2-203]. The Burgers vector reaction of this SF is 1/3[1-100] +

60

$1/2[0001] \rightarrow 1/6[2\text{-}203]$, and the length of each Burgers vectors are $a/\sqrt{3}$ for $b=1/3[1\text{-}100]$ and $c/2$ for $b=1/2[0001]$. It explains well why the SD density reduced much faster than the ED density.

3-8. Summary and conclusions

The role of an IT-GaN grown at 900 $^{\circ}$C was investigated. HVPE GaN film grown on IT-GaN showed better crystal quality with smooth surface, negligible residual strain, and stronger luminescence intensity than the GaN without it. Cross-sectional CL revealed that the remarkable improvement of crystal quality was achieved during the growth of IT-GaN. In addition, IT-GaN contains high density SFs, which imposes that the TD reduction is related with SF which was confirmed by TEM results. We have observed the ED and SD density variation along with the growth direction. The SD density decreased fast during the growth of IT-GaN due to the interaction with SF.

References

[1] A. Sakai, H. Sunakawa and A. Usui, Appl. Phys. Lett. 73 (1998) 481.

[2] S. W. Lee, J.-S. Ha, H.-J. Lee, H.-J. Lee, H. Goto, T. Hanada, T. Goto, K. Fujii, M. W. Cho and T. Yao, Appl. Phys. Lett. 94(2009) 082105.

[3] G. Chen, J. Chyi, C. Chan, C. Hou, C. Chen and M. Chang, Appl. Phys. Lett. 91 (2007) 261910.

[4] H.J. Lee, J.S. Ha, T. Yao, C.K. Kim, S.K. Hong, J.H. Chang, J.W. Lee and J.Y. Lee, Cryst. Growth Des. 9 (2009) 2877.

[5] Y. J. Cho, J. S. Ha, M. N. Jung, H. J. Lee, S. H. Park, J. S. Park, K. Fujii, R. Toba, S. N. Yi, G. S. Kil and J. H. Chang, T. Yao, J. Cryst. Growth 312 (2010) 1693.

[6] D. K. Kim, Sol. Stat. Elect. 51 (2007) 1005.

[7] E. Dimakis, J.Z. Domagala, A. Delimitis, Ph. Komninou, A. Adikimenakis, E. Iliopoulos and A. Georgakilas, Superlattices and Microstructures 40 (2006) 246.

[8] D. Cherns, W. T. Young, J. W. Steeds, F. A. Ponce and S. Nakamura, J. Cryst. Growth 178 (1997) 201.

[9] J. S. Ha, H. J. Lee, S. W. Lee, H. J. Lee, S. H. Lee, H. Goto, M. W. Cho, T. Yao, S. K. Hong, R. Toba and J. W. Lee, J. Y. Lee, Appl. Phys. Lett. 92 (2008) 091906.

[10] F. K. Yam, Z. Hassan and S. S. Ng, Thin Solid Films 515 (2007) 3469.

[11] A. Ubukata, K. Ikenaga, N. Akutsu, A. Yamaguchi, K. Matsumoto, T. Yamazaki and T. Egawa, J. Cryst. Growth 298 (2007) 198.

[12] C.W. Liu and V. Venkataraman, Mat. Che. Phys. 49 (1997) 29.

[13] J. Schreiber, S. Hildebrandt, H. Uniewski and V. Bechstein, Mat. Sci. Eng. B42 (1996) 24.

[14] C. Stampfl, and C. G. Van de Walle, Phy. Rev. B 57 (1998) R15052.

[15] R. Liu, A. Bell, F. A. Ponce, C. Q. Chen, J. W. Tang, and M. A. Khan, Appl. Phys. Lett. 86 021908 (2005).

[16] M. A. Reshchikov and H. Morkoç, J. Appl. Lett. 97 (2005) 061301.

[17] T.B. Wei, Q. Hu, R.F. Duan, X.C. Wei, Z.Q. Huo, J.X. Wang, Y.P. Zeng, G.H. Wang and J.M. Li, J. Cryst. Growth 311 (2009) 4153.

[18] Y. J. Sun, O. Brandt, U. Jahn, T. Y. Liu, A. Trampert, S. Cronenberg, S. Dhar and K. H. Ploog, J. Appl. Phys. 92 (2002) 5714.

[19] W. J. Bartels, J. Vac. Sci. Technol. B1 (1983) 338.

[20] Y. T. Rebane, Y. G. Shreter and M. Albrecht, Phys. Stat. Sol. (a) 164 (1997) 141.

Chapter 4. HVPE Growth of reduced defect density nonpolar GaN

4-1. Introduction

Group III-nitrides have a non-centrosymmetric structure with no center of inversion, which builds a spontaneous and piezoelectric polarization into the film. With group III-nitride heterostructures grown along the *c*-axis direction, the discontinuity of polarization at the interface induces a large internal electric field, which significantly deteriorates the efficiency of optoelectronic devices [1]. Thus, the epitaxial growth of GaN with non-polar crystal planes, such as an *a*-plane (*a*-GaN) or an *m*-planeGaN (*m*-GaN), were considered as alternatives [2,3]. However, non-polar devices suffer considerably from problems such as poor electrical and optical properties mainly due to the difficulty of growing a high-quality, non-polar GaN film [4]. Many reports have documented the hetero-epitaxial growth of *m*-GaN films on *m*-GaN [5], *m*-plane SiC [6], (100) LiAlO$_2$ [7], *m*-plane ZnO [8], and *m*-plane sapphire(*m*-sapphire) substrates [9,10]. Although an *m*-GaN substrate provided the best results, the *m*-sapphire is still an attractive substrate for the growth of *m*-GaN films, because it is cost-effective, chemically and thermally stable, and is available on a large scale compared with other substrates. Despite their advantages, however, the critical problems, such as rough surface morphology and poor crystal quality, have persisted for *m*-GaN films grown directly on an *m*-sapphire.

64

In the present study, an attempt was made to grow *m*-GaN film on a vicinal *m*-sapphire substrate. Vicinal surface epitaxy has been reported as a promising technique that can significantly improve the crystalline quality of nitrides grown on sapphire [11,12]. Matsuoka *et al*. have reported that vicinal surface epitaxy improved the quality of *c*-plane GaN by optimizing the inclination angle and employing optimal growth conditions [13]. However, there has been scant research in this area with respect to the use of *m*-GaN film.

In the present chapter, the relationship between inclination directions of a substrate and the crystal quality of *m*-GaN films was investigated, and an attempt was made to explain the results by proposing a simple stacking model that could reveal the relationship between a structural defect and an inclination direction.

4-2. Experimental details

The *m*-GaN films were grown by hydride vapor phase epitaxy (HVPE) on three different types of *m*-sapphire substrates. m_a-GaN sample was grown on *m*-sapphire inclined 2° toward the *a*-axis direction. m_{just}-GaN sample was grown on an *m*-sapphire substrate without artificial inclination. m_c-GaN sample was grown on an *m*-sapphire substrate inclined 2° toward the *c*-axis direction. The growth temperature was 1,040 $^{\circ}$C for all samples, and the thickness was maintained at 45 μm. The surface morphology was analyzed using an optical microscope. To characterize the optical properties, low temperature (12 K) photoluminescence (PL) and temperature

65

dependence PLwere measured using the 325nm line of a He-Cd laser as an excitation light source. A plane-view transmission electron microscope (TEM), a high-resolution TEM, and high-resolution X-ray diffraction (HRXRD) were used to analyze the structural properties. Also, a ball-and-stick atomic model was proposed to explain the effect when using a vicinal m-plane sapphire substrate.

4-3. Surface morphology and structure evaluation
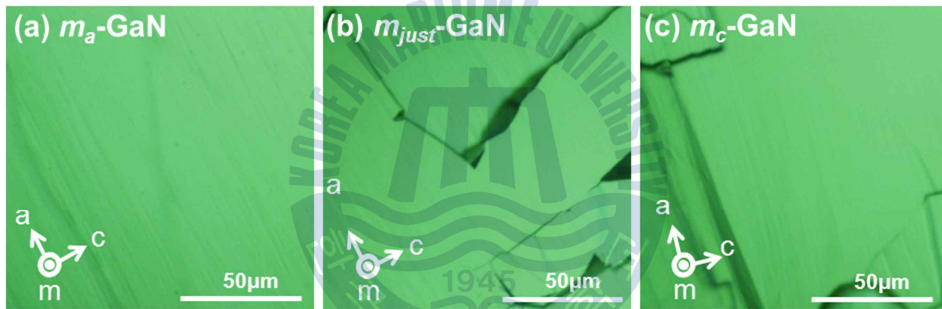
Fig. 4.1 Optical microscopy images of m-GaN grownon various m-sapphires inclined in the (a) a-axis direction (m_a-GaN), (b) without inclination (m_{just}-GaN), and (c) in the$c$-axisdirection (m_c-GaN).

Fig. 4.1 shows the optical microscope images of the m-GaN samples. The m_a–GaN had a smooth surface, as shown in Fig.4.1(a). Fig.4.1(b) and (c) show the respective surface morphologies of m_{just}–GaN and m_c–GaN. These results demonstrated that the inclination direction is closely related to surface morphology.

However, a considerable difference was not observed between m_{just}–GaN and m_c–GaN.

It was well known that the surface morphology of a film is closely related to its lattice defect [14]. Hence, the results shownin Fig. 4.1 imply that the structural quality of m-GaN films is also closely correlated to the inclination direction of substrates.

The samples also were characterized using high-resolution X-ray diffraction. For the present study, (1-100) omega rocking curves were measured along with the a-axis and c-axis directions, as listed in Table 4. 1. The m_a-GaN sample showed full width at half maximum (FWHM) values that were the narrowest for both directions.

TABLE 4.1. The FWHM values of x-ray rocking curve for m-GaN films.

Samples	FWHM(arcsec)	
	X-ray // a-axis direction	X-ray // c-axis direction
m_a-GaN	504	4104
m_{just}-GaN	712	5364
m_c-GaN	695	5328

4-4. Optical properties

Fig. 4.2 shows the PL spectra at 12 K. Broad luminescence bands with multiple peaks were seen in all samples. The luminescence band was basically composed of three major emission lines centered at 3.42 eV, 3.38eV, and 3.34eV. Those emission lines seemed to be related to the structural defects in GaN [15]. The results from various studieshaveassigned those peaks to the recombination exciton that is bound to structural defects such as the stacking fault (SF) [16-18]. Consequently, the PL spectra revealed that the carrier recombination process in these samples was strongly dependent on the structural defects.

Clarifying the origin of those emission lines would require further study, so the peaks were tentatively assigned according to the results reported in previous studies. The peaks at 3.42 eV and 3.34 eVwere assigned to excitonic emissions related to type-I and II basal-plane stacking faults (BSF) [19, 20], respectively, while a definite origin of the peak at 3.38 eV is not known yet. Interesting behavior was observed from the BSF-related emission lines.

The intensity of the 3.34 eV emission decreased with the inclination from the*c* tothe*a* direction, while the intensity of the 3.42 eV emission increased. It was a curiosityas to why the intensities moved in opposite directions.
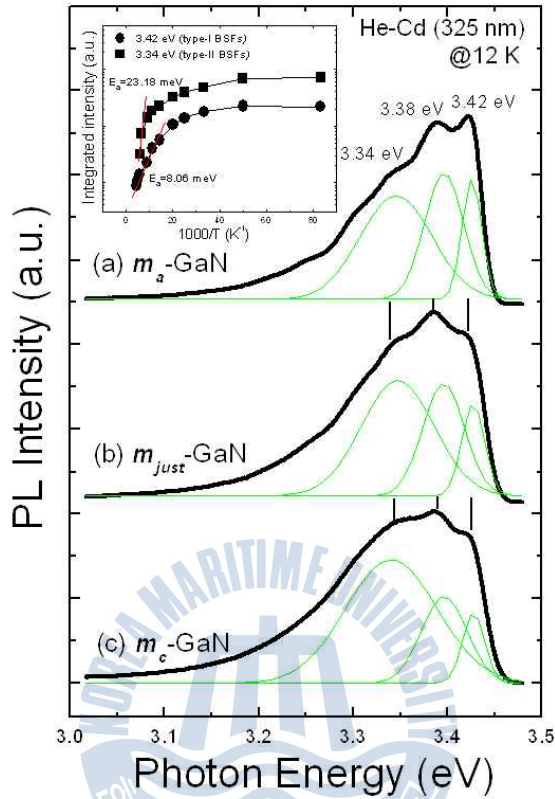
Fig. 4.2 PL spectra of *m*-GaN films grown on various *m*-sapphires.(a) m_a-GaN, (b) m_{just}-GaN, and (c) m_c-GaN. The inset shows the temperature dependence of integrated PL intensities of the peaks at 3.34 eV and 3.42 eV for m_a-GaN.

The presumption was that the difference was related to the types of stacking faults. Stampfl and Van de Walle reported the energies of stacking faults in nitrides. The calculated formation energy of a type-II basal stacking fault (BSF) is 2.4 times larger than a type-I BSF in GaN [21]. Hence, a type-I BSF should be the most common structural defect for GaN. However, a type-II BSF would be more effective in terms of reduction the total energy of a crystal. When the thickness of

69

the*m*-GaN films is the same, a decrease of type-I BSF density should increase the density of a type-II BSF in the film.

The inset of Fig. 4.2 shows the temperature dependence of the integrated intensity of each peak at 3.42 eV and 3.34 eV. From an Arrhenius plot of peak intensities, activation energies of 8.06 meV and 23.18 meV were extracted for the peaks at 3.42 eV and 3.34 eV, respectively. These results did not quantitatively correspond with the reported activation energy values of 13 meV [15] and 30 meV [16] for type-I and type-II BSFs, respectively. However, these results imply that the origins of each peak have considerably different energetic states.

4-5. TEM measurement

Figs. 4.3 (a)-(c) show the plane view TEM images of the three samples. The insets are diffraction patterns of each image. The dark strips in those images are considered to be caused by the stacking faults (SF). Only the SFs with a direction perpendicular to the *c*-axis of the film were observed in all samples. The direction of SFs indicated that those are BSFs. Also, the m_a-GaN sample showed the lowest density for SF, which corresponded well with the surface morphology and PL results.

High resolution TEM (HRTEM) was used to observe the details of the BSF. HRTEM images of the BSF for m_a-GaN are shown in Figs. 4. 3 (d)-(e). Fig. 3 (d) shows that the BSF is a single SF in the basal plane (*c*-plane), rather than blocks of

70

cubic material embedded in a wurtzite-structure matrix. Fig. 4.3 (e) shows a type-I BSF with the stacking sequence ABA<u>BAC</u>ACA. The lattice images of different stacking faults were analyzed for the present study, and all werefound to be type-I BSF. Nevertheless, because of the PL spectra, it was assumed that type-II BSF existed on m_a-GaN.
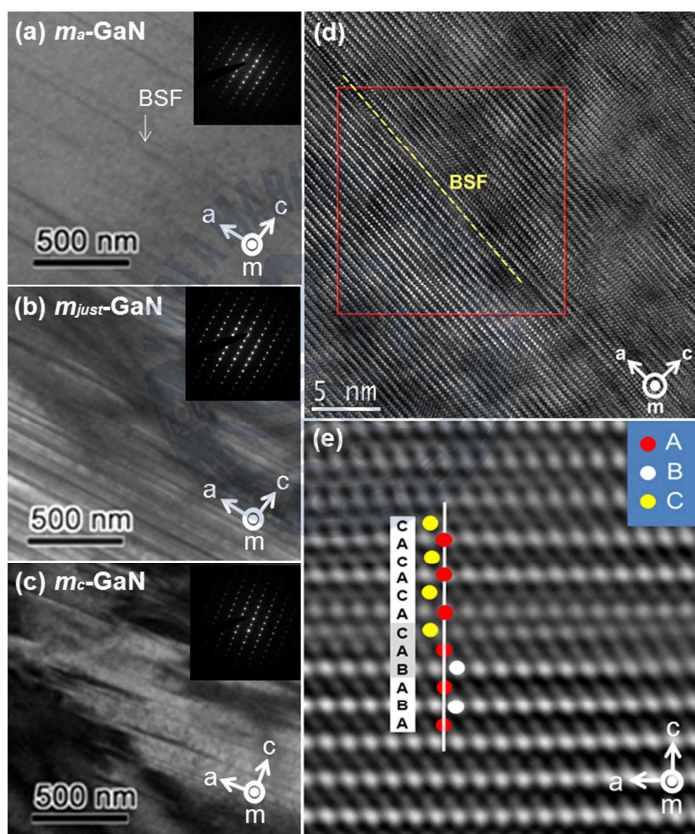

Fig. 4.3 TEM images of m-GaN films; (a) m_a-GaN, (b) m_{just}-GaN, (c) m_c-GaN (The insets show diffraction patterns of samples), HRTEM images of m_a-GaN; (d) basal-plane stacking fault, and (e) a type-I basal stacking fault of with the stacking sequence ABA<u>BAC</u>ACA.

These results indicate that the inclination direction of the substrate was strongly related to the BSF density as well as to the morphology of the *m*-GaN film.

4-6. Atomic stacking models

To explain the correlation between the inclination direction and the SF density, the simple model shown in Fig. 4.4 was proposed. Note that we just considered the crystallographic relationship like as [0001] *c*-GaN//[11-20] *m*-sapphire and [11-20] *m*-GaN//[0001] *c*-sapphire, because this regime provides less misfit strain to the film , also we confirmed this relationship by measuring the XRD pole figure plot of the samples.
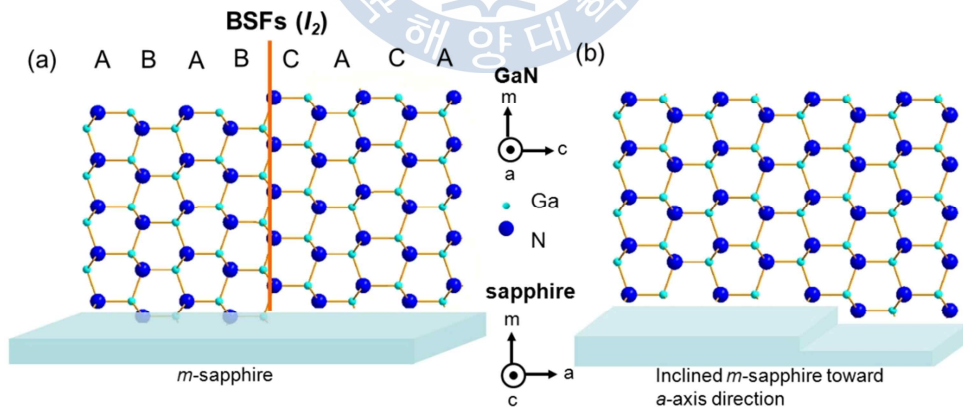

Fig. 4.4 Atomic stacking models of *m*-GaN film grown on (a) an *m*-sapphire with no inclination, and (b) an *m*-sapphire inclined in the *a*-axis direction.

Fig. 4.4 (a) shows an atomic stacking model for a type-II BSF for (with a Burgers vector of 1/3<10-10>) m-GaN grown on an m-sapphire with no inclination. This shows that a BSF causes a surface roughening with a height of 1/3ML (~0.9 Å) [22], which provides an active nucleation site and a faster nucleation rate [23]. Hence, the irregularity of the surface will increase as the growth proceeds. Fig. 4 (b) shows m-GaN grown on an inclined substrate in the a-axis direction. This is a good example of how the BSFs can be diminished by a step on the substrate surface with proper height. However, a surface inclined in the c-axis direction would have a negligible effecton the reduction of the SF density in the m-GaN film, since the dominant SF in GaN is on the basal plane.

It is worthy to noting that the compensation of the BSF by surface step is closely related with not only the step height but also the spacing between steps (i.e. terrace length). In our experiment, the ideal step height of m-sapphire inclined 2° toward the a-axis direction is estimated to be as low as 0.16 Å with a terrace length of 25.8 Å. While the displacement by a BSF is estimated to be 0.9 Å in height with a spacing of 26.5 Å [24], which was assumed from equilibrium spacing of misfits. This discussion indicates that the SF density in the m-GaN film grown on m-sapphire inclined 2° toward the a-axis direction will decrease ~17% of the m-GaN film grown on m-sapphire with no inclination in terms of the reduction of lattice deformation. Note that the observed SF density of m_a-GaN [Fig. 4. 3(a)] was 6.88 X 10^{7}/cm^2 which is 10.6 % of the SF density (6.52 X 10^{6}/cm^2) estimated from the m_{just}-GaN [Fig. 4. 3(b)].

73

4-7. Summary and conclusion

m-GaN films were grown on m-sapphire substrates with various surface inclination directions. A smooth surface and a high crystal quality as well as a low defect density were observed for m_a-GaN film. A simple atomic model was proposed to explain the reduction in BSF when using an inclined substrate.

References

[1] P. Waltereit, O. Brandt, A. Trampert, H.T. Grahn, J. Menniger, M. Ramsteiner, M. Reiche and K. H. Ploog, Nature 406 (2000) 865.

[2] C. Q. Chen, M. E. Gaevski, W. H. Sun, E. Kuokstis, J. P. Zhang, R. S. Q. Fareed, H. M. Wang, J. W. Yang, G. Simin, M. A. Khan, H. P. Maruska, D. W. Hill, M. M. C. Chou and B. Chai, Appl. Phys. Lett. 81(2002) 3194.

[3] H. M. Ng, Appl. Phys. Lett. 80 (2002) 4369.

[4] M. D. Craven, S. H. Lim, F. Wu, J. S. Speck and S. P. DenBaars, Appl. Phys. Lett. 81 (2002) 469.

[5] M. McLaurin and J. S. Speck, Phys. Stat. Sol. (RRL) 1 (2007) 110.

[6] N. F. Gardner, J. C. Kim, J. J. Wierer, Y. C. Shen and M. R. Krames, Appl. Phys. Lett. 86 (2005) 111101.

[7] P. Waltereit, O. Brandt, M. Ramsteiner, R. Uecker, P. Reiche and K. H. Ploog, J. Cryst. Growth 218 (2000) 143.

[8] A. Kobayashi, S. Kawano, Y. Kawaguchi, J. Ohta and H. Fujioka, Appl. Phys. Lett. 90 (2007) 041908.

[9] R. Armitage and H. Hirayama, Appl. Phys. Lett. 92 (2008) 092121.

[10] H. Sasaki, H. Sunakawa, N. Sumi, K. Yamamoto and A. Usui, J. Cryst. Growth 311 (2009) 2910.

[11] M. H. Xie, L. X. Zheng, S. H. Cheung, Y. F. Ng, H. Wu, S.Y. Tong and N. Ohtani, Appl. Phys. Lett. 77 (2000) 1105.

[12] J. Kato, S. Tanaka, S. Yamada and I. Suemune, Appl. Phys. Lett. 83 (2003) 1569.

[13] T. Matsuoka and E. Hagiwara, Phys. Status Solidi A 188 (2001) 485.

[14] D. K. Kim, Solid-State Electron. 51 (2007) 1005.

[15] M. A. Reshchikov and H. Morkoç, J. Appl. Phys. 97 (2005) 061301.

[16] P. P. Paskov, R. Schifano, B. Monemar, T. Paskova, S. Figge and D. Hommel, J. Appl. Lett. 98 (2005) 093519.

[17] S. Fischer, G. Steude, D. M. Hofmann, F. Kurth, F. Anders, M. Topf, B. K. Meyer, F. Bertram, M. Schmidt, J. Christen, L, Eckey, J. Holst, A. Hoffmann, B. Mensching and B. Rauschenbach, J. Cryst. Growth 189 (1998) 556.

[18] B. Bastek, F. Bertram, J. Christen, T. Wernicke, M. Weyers and M. Kneissl, Appl. Phys. Lett. 92 (2008) 212111.

[19] R. Liu, A. Bell, F. A. Ponce, C. Q. Chen, J. W. Yang and M. A. Khan, Appl. Phys. Lett. 86 (2005)021908.

[20] Y. J. Sun, O. Brandt, U. Jahn, T. Y. Liu, A. Trampert, S. Cronenberg, S. Dhar and K. H. Ploog, J. Appl. Phys. 92 (2002) 5714.

[21] C. Stampfl and C. G. Van de Walle, Phys. Rev. B 57 (1998) R15052.

[22] Ph. Ebert, L. Ivanova, S. Borisova, H. Eisele, A. Laubsch and M. Dähne, Appl. Phys. Lett. 94 (2009) 062104.

[23] M. Ichimura and J. Narayan, Mater. Sci. Eng. B 31(1995) 299.

[24] J. W. Lee, J. H. Kim, S. K. Han, S. K. Hong, J. Y. Lee, S. I. Hong and T. Yao, J. Cryst. Growth 312 (2010) 238.

Chapter 5. Summary and conclusion

This thesis will contribute to solve the critical problems of difficulty in high quality GaN film growth due to a lack of GaN bulk substrate. This thesis has introduced HVPE thick GaN film for producing GaN substrate and has suggested methods to grow high quality polar and non-polar thick GaN film. ***In the chapter 3***, the effect of a GaN buffer layer grown at 900 $^{\circ}$C (IT-GaN) on crystalline of overgrown GaN has been investigated and the role of IT-GaN on reduction of dislocation has been discussed. IT-GaN is apt to grow high quality GaN in terms of smooth surface morphology, optical properties and better crystallinity of overgrown GaN. Because threading dislocations are reduced by basal stacking faults in IT-GaN which is generated by dismantlement of perfect dislocation. ***In the chapter 4***, it is discussed that the effect of the inclination direction of vicinal *m*-plane sapphire substrate on the structural and optical properties of *m*-plane GaN (*m*-GaN) films. The inclined in the *a*-axis direction showed the highest quality and a model is proposed that shows how the surface step of a substrate can reduce the generation of stacking fault in *m*-GaN film.

As a result, the quality of HVPE GaN has been improved with reduction of

defects by suggested techniques. This thesis provides that techniques to grow high

quality HVPE thick are a great help to fabricate high efficiency GaN device by

heteroepitaxy.

Appendix A

Effect of the growth mode on the generation of defects in GaN films grown by HVPE

Introduction

GaN based III-nitride materials have been one of the most attractive materials due to their potential applications both to optical and high-power devices [1-2]. However, heteroepitaxial GaN films usually have a lot of defects, and those defects are one of main problems in the application of high efficiency devise by their non-radiative recombination [3]. Thus investigation of defects is essential

Among the various defects such as dislocation, stacking fault and pit, the pit might be the most critical defect which could considerably deteriorate the device performance by providing a leakage current path through the p-n junction [4]. Hence there have been a lot of researches on the formation mechanism and the way of reduction the pits. The pits are generated from various causes like as threading dislocation [5], stacking fault [6] and inversion domain [7]. However, the kinetic behavior of this defect related with the growth kinetics of hydride vapor phase

epitaxy (HVPE) has not been investigated well enough.

In this study, we focus on the GaN growth mode. And we characterized the effect of the growth mode on the generation of pits in GaN films grown on the pit surface.

Experimental

The GaN films were grown by hydride vapor phase epitaxy (HVPE) on GaN/sapphire templates. The 20μm thickness GaN template was grown at 1040 ^{o}C under V/III ratio of 25. Sample A was grown at 1080 ^{o}C under V/III ratio of 15 and sample B was grown at 1080 ^{o}C under V/III ratio of 40. The thicknesses of samples A and B were 30 μm and 100 μm, respectively. Scanning electron microscopy (SEM) was used to observe surface morphologies of GaN films. To characterize the optical properties, low temperature (15k) and excitation power dependence photoluminescence (PL) were measured using He-Cd laser (325nm) as the excitation source. The carrier concentration and mobility was measured by hall effect measurement with Van der Pauw configuration at room temperature. Transmission electron microscopy (TEM) was used to analyze the structural

properties of the samples.

Result and discussion

Fig. A.1(a)-(c) show plan-view SEM image of GaN template, Sample A and B.
the pit densities were estimated to be 2 X 10^{12} cm^{-2}, 9.6 X 10 cm^{-2} and 9.9 X 10^{4} cm^{-2} for GaN template, Sample A and B, respectively. Although the samples were grown on same template, Sample A showed considerably low pit density than Sample B. The surface roughness is a strong relationship with internal defect [8], it shows that Sample B had more internal defects than Sample A.
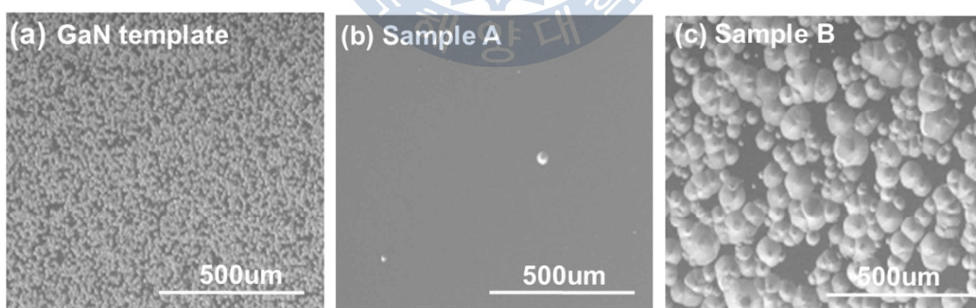

Fig. A.1 SEM images for (a) the GaN/sapphire template (20um), (b) Sample A
(30um) and (c) Sample B (100um).

There have been a lot of reports on the generation mechanism of pits. Although it

is related with various parameters such as the V/III ratio [9], growth rate [10], growth temperature [11], impurities [12], surface energy of growth front [13] and the sort of substrate, it is still very difficult to make a simple explanation which connect the cause and result directly, since those parameters are closely related with each other. Hence, we have to consider various aspects of those parameters carefully.

Epitaxial growth of group-III nitrides by means of vapor-phase epitaxy typically requires growth temperature in excess of 1000 ^{o}C [14], due to the large binding energies of the species involved. At lower temperature and at low V-III ratio, the epitaxial layers tend to grow in a faceted manner. In other words, in order to achieve smooth planar surfaces, high temperature and large V-III ratio are required [15].
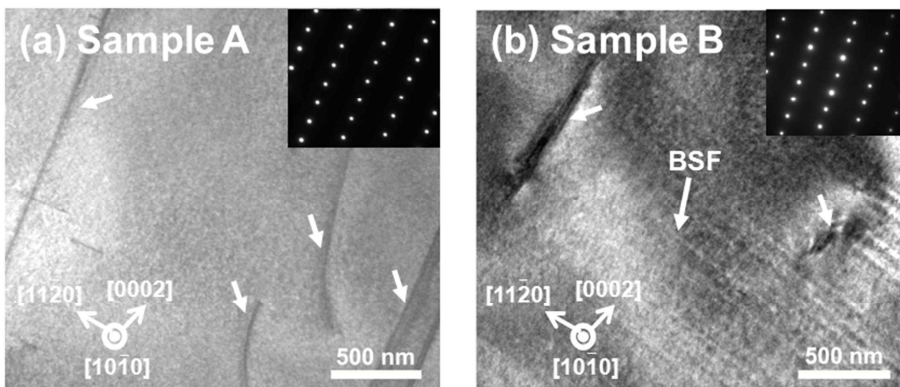

Fig. A.2 Cross-sectional TEM images of (a) Sample A and (b) Sample B. The

83

diffraction patterns of samples were shown in the inset.

In the case of smooth template surface without pit, two-dimensional growth conditions, such as high temperatures, large V/III ratio, fast growth rate, low impurities, are known to inhibit the pit formation [16]. But in the case of a rough template surface, high density defects caused by the three-dimensional growth need to be blocked the spread of defects from growth surface. Therefore, in this study, Sample A grown with small V/III ratio has a low pit density due to the growth on the high pit surface.

This is similar to the result that the high quality film is grown from the low growth temperature than the film is grown at high temperature directly, when the ZnTe homoepitaxial films were grown on rough surfaces. It is suitable for initial growth that the migration length is limited in case of high density of nucleation site on growth surface [17]

TEM measurement was performed to analyze atomic structure such as dislocation and stacking fault. Samples for TEM measurement were prepared by focused ion beam. Fig. A.2 shows cross-sectional TEM images of the samples. The insets are diffraction patterns of the each image. White arrows indicate dislocations

84

in Fig. A.2 (a) and (b). There are only dislocations in Sample A but Sample B has

basal stacking fault (BSF) as well as dislocation. This result corresponds to the

explanation that Sample B with rough surface has a high density of inter defects.

In Fig. A.3, low-temperature PL spectra of the two samples are shown. All

spectra are revealed same emissions at 3.47 eV, 3.37 eV, 3.26 eV, 3.17 eV and 3.08

eV, which are assigned donor bound exciton (D^0X), LO phonon replica of D^0X

(D^0X-LO), donor-acceptor pair in hexagonal GaN (h-DAP), DAP in cubic GaN (c-

DAP), and LO phonon replica of DAP (DAP-LO), respectively [18]. The emission

at 3.17 eV is related with cubic phase GaN and it was expected that the cubic phase

was due to BSFs of the film in Fig. A.2 (b) [19]. The DAP related emissions were

strong in Sample B. DAP emission is related impurity. This result indicates that

Sample B have a higher impurity density than sample A.

The growth rate is dependent on V/III ratio. Typically, back ground impurity

increase in a low growth rate [20]. However, in this study, back ground impurity is

higher while the growth rate become high. It is considered that the facet of pit has a

high incorporation coefficient [21]. Actually, carrier concentrations were 4.45 X

10^{18} cm^{-3} and 4.07 X 10^{19} cm^{-3} for Sample A and B, respectively, in Hall effect
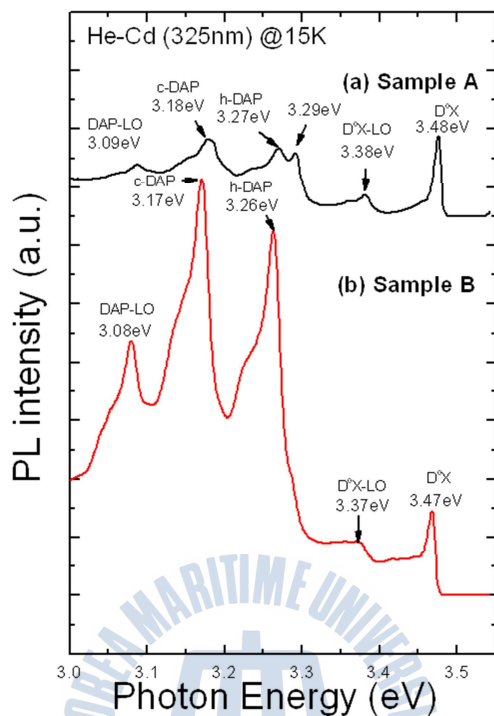
measurement.

85

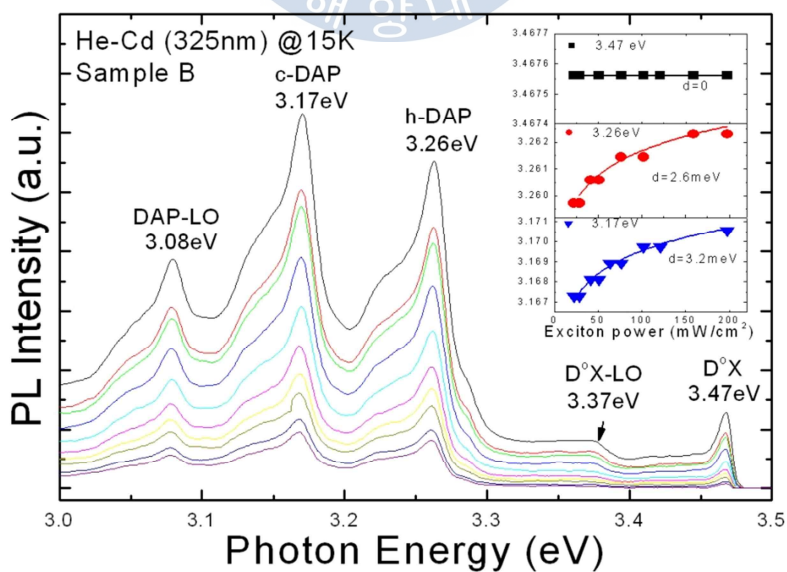Fig. A.3 PL spectra for the GaN films at 15K (a) Sample A and (b) Sample B

Fig. A.4. The excitation power dependence PL spectra of Sample B. The excitation power intensity versus peak energy was shown inset.

The excitation power dependence PL was performed to investigate properties of emissions in the exciton power density ranged from 20mW/cm^2 to 200mW/cm^2. Fig. A.4 shows the excitation power dependence of PL spectra of Sample B. Inset shows the dependence of the PL emission band peak energy as a function of excitation laser intensity. The 3.47 eV emission shows no shift but 3.26 eV and 3.17 eV emissions show blue shifts for 2.6 meV and 3.2 meV, respectively. In DAP recombination, photo excited carriers trapped at ionized donors and acceptors recombine radiatively. For DAP transition, the peak energy is a function of an interpair distance r through the initial and final state interaction between the donor and acceptor [22]:

$$E_{DA} = E_g - (E_A + E_D) + \frac{c^2}{\varepsilon r} \qquad (1)$$

where E_g is the band gap energy, E_D and E_A are the donor and acceptor binding energies, ε is the dielectric constant. During the increasing of the excitation power, r decreased by increased photon density. Thus DAP shows a blueshift with increasing the excitation power.

87

Summary and Conclusion

In conclusion, we have reported the effect of growth mode on the generation of pits in GaN film. The GaN sample grown at high V/III ratio has a high pit density, strong intensities of DAP related emissions, high impurity and BSFs density. In contrast, the GaN sample grown at low V/III ratio has a smooth surface and low defects density inside film. These results suggest that three-dimensional growth by a low V/III ratio leads to provide a smooth surface and a low defects density by blocking the spread of the defects from growth surface when the GaN film grown on the rough surface.
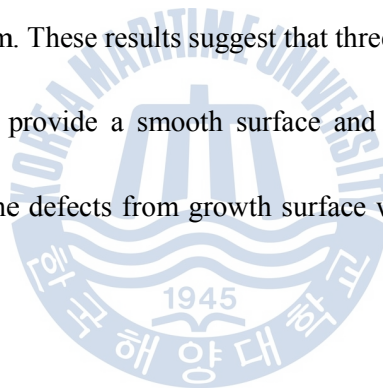
References

[1] S. Nakamura, M. Senoh, T. Mukai, Appl. Phys. Lett. 62 (1993) 2390

[2] M. Asif Khan, J. Kuznia, D. Olson, W. Schaff, J. Burm, M. Shur, Appl. Phys. Lett. 65 (1994) 1121

[3] M.F. Schubert, S. Chhajed, J.K. Kim, E.F. Schubert, Appl. Phys. Lett. 91 (2007) 2311147

[4] X. A. Cao, J. A. Teetsov, F. Shahedipour-Sandvik, S. D. Arthur, J. Cryst. Growth 264 (2004) 172

[5] Z.L. Weber, Y. Chen, S. Runimov, J. Washburn Phy. Rev. Lett. 79 (1997) 2835

[6] H.K. Cho, J.Y. Lee, G.M. Yang, C.S. Kim, Appl. Phys. Lett. 79 (2001) 215

[7] V. Potin, P. Ruterana, G. Nouet, Mat. Sci. Eng. B 59 (1999) 173

[8] M. Jamil, E. Irissou, J.R. Grandusky, V. Jindal, F. Shahedipour-Sandvik, Phys. Stat. Sol. (c) 3 (2006) 1787

[9] M. Ishida, M. Ogawa, K. Orita, O. Imafuji, M. Yuri, T. Sugino, K. Itoh, J. Cryst. Growth 221 (2000) 345

[10] T. Paskova, E.M. Goldys, R. Yakimova, E.B. Svedberg, A. Henry, B. Monemar, J. Cryst. Growth 208, (2000) 18

[11] K.S. Son, D. Kim, H.K. Cho, K. Lee, S. Kim, K. Park, J. Kim, Phys. Stat. Sol.

(c) 0 (2003) 2095

[12] Z. Liliental-Webber, J. Electron. Microscopy 49 (2000) 339

[13] E. Valcheva, T. Paskova, B. Monema, J. Cryst. Growth 255 (2003) 19

[14] Z.Y. Zhai, X.S. Wu, H.L. Cai, X.M. Lu, J.H. Hao, J. Gao, W.S. Tan, Q.J. Jia, H.H. Wang, Y.Z. Wang, J. Phys. D: Appl. Phys. 42 (2009) 105307

[15] A. Hangleiter, F. Hitzel, C. Netzel, D. Fuhrmann, U. Rossow, G. Ade, P. Hinze, Phys. Rev. Lett. 95 (2005) 127402

[16] Y. Golan, X. H. Wu, J. S. Speck, R. P. Vaudo, V. M. Phanse Appl. Phys. Lett. 73 (1998) 3090

[17] J. H. Chang, M. W. Cho, H. M. Wang, H. Wenisch, T. Hanada, T. Yao, Appl. Phys. Lett. 77 (2000) 1256

[18] M.A. Reshchikov, H. Morkoc, J. Appl. Phys. 97 (2005) 61301

[19] H. Kim, T.G. Andersson, J.-M. Chauveau, A. Trampert, Appl. Phys. Lett. 81 (2002)

[20] O. Kryliouk, M. Reed, T. Dann, T. Anderson, Bruce Chai, Mat. Sci. Eng. B59 (1999) 6

[21] K. Zywietz, J. Neugebauer, M. Scheffler, Appl. Phys. Lett. 74 (1999) 1695

[22] J. Wu, H. Yaguchi, K. Onabe, R. Ito, Appl. Phys. Lett. 71 (1997) 2067

List of publications & presentations

International publications

<u>Youngji Cho</u>, Jun-Seok Ha, Mina Jung, Hyun-Jae Lee, Seunghwan Park, Jinsub Park, Katsushi Fujii, Ryuichi Toba, Samnyung Yi, Gyung-Suk Kil, Jiho Chang, Takafumi Yao, " The impact of an intermediate temperature buffer on the growth of GaN on an AlN template by hydride vapor phase epitaxy", **Journal of Crystal Growth**, 312 (2010) 1693

Seungjun Oh, Mina Jung, Jieun Koo, <u>Youngji Cho</u>, Sungkuk Choi, Samnyung Yi; Gyungsuk Kil, Jiho Chang, "The mechanism of ZnO nanorod growth by vapor phase transportation", **Physica E**, 42 (2010) 2285

<u>Youngji Cho</u>, Sungkuk Choi, Gyung-Suk Kil, Hyun-Jae Lee, Takafumi Yao, Jun-Mo Yang, JunghoYoo, Jangwoo Kwon, Jiho Chang, "Effects of the inclination direction of vicinal m-plane sapphire substrates on the crystal quality of m-plane GaN film", **Journal of Crystal Growth**, 325 (2011) 85

Domestic publications

<u>조영지</u>, 이현재, 이웅, T. Sekiguchi, T. Yao, 양준모, 유정호, 장지호, "성장모드가 HVPE GaN 후막의 결함 형성에 미치는 영향", 한국해양대학교 부설 산업기술연구소, 28 (2011) 77

조유진, <u>조영지</u>, 유진엽, 구지은, 최성국, 장지호, 이상태, 이원재, "열처리를 통한 (11-20) ZnO 기판의 표면 형상 및 광학적 특성의 변화에 대한 고찰", **새물리**, 61 (2011) 311

구지은, <u>조영지</u>, 장지호, 박승환, 이웅, 이효종, 이상태, "고온가압 열처리법을 이용한 ITO 의 전기적 특성 개선과 가스센서 응용에 관한 연구", **새물리**, 61 (2011) 311

Presentations in the international conferences

Jiho Chang, Hyunjae Lee, Mina Jung, <u>Youngji Cho</u>, Bonheun Koo, Bonheun Koo, Hyojong Lee, Takafumi Yao, "Growth of O- and Zn-polar ZnO films by DC magnetron sputtering", International Symposium on Compound Semiconductors, Kagawa, Japan, June, 2010.

M. N. Jung, S. K. Choi, J. E. Koo, <u>Y. J. Cho</u>, S. N. Yi, G. S. Kil, S. T. Lee, H. J. Lee, T. Yao, d. C. Oh, J. H. Chang, "Decrease of Aluminum concentration during the synthesis of Al-doped ZnO nanostructures at high temperature", International Coference on Molecular Electronics and Devices, Suncheon, Korea, May, 2010.

Jiho Chang, Mina Jung, Hyunjae Lee, <u>Youngji Cho</u>, Yujin Cho, JinyeopYoo, Sungguk Choi, Takafumi Yao, "Growth and characterization of single crystalline Zn-polar ZnO films by sputtering for the application to a template for GaN",

International Workshop on Znic Oxide and Related Materials, Changchun, China, August, 2010.

Youngji Cho, Hyun-Jae Lee, Woong Lee, Takashi Sekiguchi, Takafumi Yao, JunghoYoo, Jun-mo Yang, Jiho Chang, "The role of an intermediate temperature buffer in the improvement of crystallinity of HVPE GaN,", The 15th International Symposium on the Physics of Semiconductors and Applications, Jeju, Korea, July, 2011

Youngji Cho, Joonseok Ha, Hyun-Jae Lee, Takafumi Yao, Woong Lee, Takashi Sekiguch, Ryuichi Toba, Jun-Mo Yang, Jungho Yoo, Jiho Chang, "The role of an intermediate temperature buffer on the improvement of crystallinity of HVPE GaN", The 72nd Autumn Meeting of the Japan Society of Applied Physics, Yamagata, Japan, August, 2011

Presentations in the Domestic conferences

조영지, 정미나, 주미연, 김시영, 구지은, 하준석, 이현재, 박승환, 박진섭, YAO Takafumi, TOBA Ryuichi, 장지호, "AlN template 상의 Hydride Vapor Phase Epitaxy 를 이용한 GaN 성장 시 중간층의 역할에 관한 연구" 한국물리학회 봄 학술발표대회, 2009 년 4 월

조영지, 정미나, 장지호, 이현재, 하준석, "HVPE 법으로 GaN 성장 시 버퍼 층의 유무에 따른 박막 내 잔류 응력의 차이에 관한 고찰", LED 반도체 조명학회, 2009 년 10 월

오승준, 조영지, 김시영, 구지은, 정미나, Kensho Okamoto, 장지호, "LED-LED 광•전 하이브리드 통신시스템의 구현", 2009 LED 반도체 조명학회, 2009 년 10 월

조영지, 정미나, 이현재, 하준석, Takafumi Yao, 장지호, "HVPE 법으로 GaN 성장시 버퍼층의 유무에 따른 후막의 결정성 변화에 관한 연구", 한국물리학회 부산경남울산지부 제 54 회 학술발표회, 2009 년 12 월

조영지, 정미나, 이현재, 최성국, Takafumi Yao, 이웅, 장지호 "성장양식의 변화에 따른 HVPE 로 성장한 GaN 의 특성 변화에 관한 연구", 한국물리학회 봄학술발표대회, 2010 년 4 월

장지호, 조유진, 조영지, 구지은, 최성국, 정미나 " C-plan 과 A-plan bulk ZnO 기판의 발광 특성의 차이에 관한 연구", 한국물리학회 봄학술발표대회, 2010 년 4 월

최성국, <u>조영지</u>, 이현재, T. Yao, 한주섭, 길경석, 장지호, "HVPE growth of m-plane GaN on vicinal surface sapphire substrates", LED, 반도체 조명학회 국내학술대회, 2010 년 8 월

조유진, 최성국, <u>조영지</u>, 이웅, 이병우, 이상태, 장지호, "스크린 프린팅 방법으로 제작한 전계방출형 발광소자의 UV 발광특성에 대한 연구", LED, 반도체 조명학회 국내학술대회, 2011 년 8 월

<u>조영지</u>, 하준석, 이현재, Katsuchi Fujii, Takafumi Yao, 이웅, Takashi Sekiguchi, 양준모, 유정호, 장지호, "중간 온도에서 성장한 버퍼층을 이용한 HVPE GaN 후막 내 결함 밀도의 감소 방법에 대한 연구", LED, 반도체 조명학회 국내학술대회, 2011 년 8 월